MEDJ

Volume: 40 Issue: 1 March 2025

MEDENIYET MEDICAL JOURNAL

THE OFFICAL JOURNAL OF ISTANBUL MEDENIYET UNIVERSITY FACULTY OF MEDICINE

Formerly Göztepe Tıp Dergisi

ISSN 2149-2042
E-ISSN 2149-4606

www.medeniyetmedicaljournal.org

ISSN 2149-2042
E-ISSN 2149-4606

MEDENIYET MEDICAL JOURNAL

Formerly Göztepe Tıp Dergisi

Year 2025
Volume 40
Issue 1

www.medeniyetmedicaljournal.org

Owner
Dean, Sadrettin PENÇE
Istanbul Medeniyet University Faculty of Medicine

Editor in Chief
M. Tayyar KALCIOĞLU
Department of Otorhinolaryngology, Istanbul Medeniyet University
mtkalcioglu@hotmail.com
ORCID: 0000-0002-6803-5467

Assistant Editors
Alpertunga KARA
Department of History of Medicine and Medical Ethics, Istanbul Medeniyet University, Türkiye
alpertunga.kara@medeniyet.edu.tr
ORCID: 0000-0002-2031-3042

Nazan AKSOY
Department of Pathology Saglik Bilimleri University, Türkiye
aksnaz@yahoo.com
ORCID: 0000-0002-9585-5567

Responsible Manager
M. Tayyar KALCIOĞLU

Administrative Office
Istanbul Medeniyet University Dumlupınar Mahallesi, D-100 Karayolu No:98, 34000 Kadıköy, Istanbul, Türkiye

Publication type: Periodical

Finance: Istanbul Medeniyet University Scientific Research Fund

Publisher
Galenos Publishing House
Address: Molla Gürani Mah. Kaçamak Sk. No: 21/1 34093 Istanbul, Türkiye
Phone: +90 (530) 177 30 97
E-mail: info@galenos.com.tr/yayin@galenos.com.tr
Web: www.galenos.com.tr

Printing at:
Son Sürat Daktilo Dijital Baskı San. Tic. Ltd. Şti.
Gayrettepe Mah. Yıldızposta Cad. Evren Sitesi A Blok No: 32 D: 1-3 34349 Beşiktaş/Istanbul
Phone: +90 212 288 45 75

Printing Date: March 2025

International scientific journal published quarterly.

Medeniyet Medical Journal is the official journal of Istanbul Medeniyet University

It is published four times a year (March, June, September, December).

MEDJ is an open Access, free and peer-reviewed journal

PubMed Abbreviation: Medeni Med J

"Please refer to the journal's webpage (**https://medeniyetmedicaljournal.org/jvis.aspx**) for "Publication Policy", "Instructions to Authors" and "Aims and Scope".

The Medeniyet Medical Journal and/or its editors are members of ICMJE, COPE, WAME, CSE and EASE, and follow their recommendations.

The Medeniyet Medical Journal is indexed in **Emerging Sources Citation Index (Web of Science), PubMed/MEDLINE, PubMed Central, Scopus, EBSCO Academic Search Complete, i-Journals, J-Gate, Türk Medline, Türkiye Atıf Dizini** and **TÜBİTAK ULAKBİM TR Index**.

The journal is printed on an acid-free paper and published electronically.

Owner: ISTANBUL MEDENİYET UNIVERSITY FACULTY OF MEDICINE

Responsible Manager: M. Tayyar KALCIOGLU

www.medeniyetmedicaljournal.org

International Advisory Board

MEDJ

International Advisory Board

Contents

DOI: 10.4274/MMJ.galenos.2025.34783
Medeni Med J 2025;40:1-11

Original Article

Biomarkers of the Complement System in Cancer

Kanserde Kompleman Sisteminin Biyobelirteçleri

Elif KUBAT OKTEM

Istanbul Medeniyet University Faculty of Engineering and Natural Sciences, Department of Molecular Biology and Genetics, Istanbul, Türkiye

ABSTRACT

Objective: Cancer is a disease characterized by an unregulated division of abnormal cells in the body. The discovery of oncogenes and tumor suppressor genes has paved the way for the targeted use of individual biomarkers and proteins in cancer therapy. The signaling pathways in cells are closely linked, and research into these connections would lead to more precise personalized treatments for cancer. An imbalance in the complement system is associated with the development and progression of cancer. Comparable variations in gene expression and common complement biomarkers in different cancer types are poorly understood. This study aims to gain insights into biomarkers linking the complement system to carcinogenesis.

Methods: Clinical and transcriptome data from the cancer genome atlas were used to analyze differentially expressed genes involved in the complement system in different cancer types. Various bioinformatics and machine learning techniques were used to suggest complement pathway-related carcinogenesis biomarkers.

Results: This study provides a comprehensive elucidation of component 7 (C7), complement factor-D (CFD), interleukin-11 (IL11), apolipoprotein C1 (APOC1), and integrin binding sialic acid protein (IBSP) proteins as common biomarkers associated with the complement system in cancer and highlights the diagnostic and prognostic potential of these biomarkers.

Conclusions: These biomarkers would pave the way for targeted cancer treatments in the context of precision medicine.

Keywords: Neoplasms, transcriptome, systems biology, complement system proteins

ÖZ

Amaç: Kanser, vücutta anormal hücrelerin kontrolsüz bölünmesiyle karakterize edilen bir hastalıktır. Onkogenlerin ve tümör baskılayıcı genlerin keşfi, kanser tedavisinde bireysel biyobelirteçlerin ve proteinlerin hedefe yönelik kullanımına olanak sağlamıştır. Hücrelerdeki sinyal yolları birbirleriyle yakından ilişkilidir ve bu bağlantılar üzerindeki araştırmalar, kanser için daha hassas kişiselleştirilmiş tedaviler geliştirilmesine yol açabilir. Kompleman sistemi dengesizliği, kanserin gelişimi ve ilerlemesiyle ilişkilidir. Farklı kanser türlerinde gen ekspresyonundaki benzer varyasyonlar ve ortak kompleman biyobelirteçleri hakkında bilgiler sınırlıdır. Bu çalışmada, kompleman sistemini karsinogenezle ilişkilendiren biyobelirteçler hakkında bilgi edinilmesi amaçlanmıştır.

Yöntemler: Kanser genom atlasından elde edilen klinik ve transkriptom verileri, farklı kanser türlerinde kompleman sistemiyle ilişkili farklı şekilde ifade edilen genlerin analizinde kullanılmıştır. Çeşitli biyoinformatik ve makine öğrenimi teknikleri, kompleman yolu ile ilgili karsinogenez biyobelirteçlerini önermek için kullanılmıştır.

Bulgular: Bu çalışma, component 7 (C7), complement factor-D (CF-D), interleukin-11 (IL-11), apolipoprotein C1 (APOC1) ve integrin-binding siyalik asit (IBSP) proteinlerini kanserde kompleman sistemiyle ilişkili ortak biyobelirteçler olarak kapsamlı bir şekilde ortaya koymakta ve bu biyobelirteçlerin tanısal ve prognostik potansiyelini vurgulamaktadır.

Sonuçlar: Bu biyobelirteçler, hassas tıp bağlamında hedefe yönelik kanser tedavilerine olanak sağlayacaktır.

Anahtar kelimeler: Neoplazmlar, transkriptom, sistem biyolojisi, kompleman sistemi proteinleri

INTRODUCTION

Cancer is a disease characterized by an unregulated division of abnormal cells in the body. While chemotherapy and surgery were initially the only options for the treatment of tumors, the identification of tumor suppressor genes and oncogenes, has contributed to the notion that individual biomarkers can be targeted for cancer treatment. Current developments in multi-omics analysis and next-generation sequencing have shown that signaling pathways in cells are tightly linked and create intricate connections.

The integrity of the immune system is crucial for the detection and elimination of cancer cells, through a dynamic mechanism that balances immune evasion and protection[1]. The complement system is a crucial aspect of both adaptive and innate immunity and consists of membrane-bound, soluble, and intracellular proteins[2]. Despite some studies in the literature (reviewed in[3]),

Address for Correspondence: E. Kubat Oktem, Istanbul Medeniyet University Faculty of Medicine, Department of Engineering and Natural Sciences, Division of Molecular Biology and Genetics, Istanbul, Türkiye
E-mail: elifkubat.oktem@medeniyet.edu.tr **ORCID ID:** orcid.org/0000-0003-0913-8527

Cite as: Kubat Oktem E. Biomarkers of the complement system in cancer. Medeni Med J. 2025;40:1-11

Received: 12 December 2024
Accepted: 06 February 2025
Epub: 11 March 2025
Published: 28 March 2025

not much is known about comparable changes in gene expression and biomarkers of the complement system in different types of cancer.

The use of biomarkers to individualize medical treatments is an instrument of precision medicine[4]. To this end, clinical and transcriptome data from nine distinct cancer types were utilized to investigate differentially expressed genes associated with the complement system, aiming to gain insights into biomarkers linking the complement system to carcinogenesis in this study. The study design is illustrated in Figure 1. This study also provides a comprehensive elucidation of the common biomarkers associated with the complement system in these cancers and highlights the potential of these biomarkers. The common biomarkers associated with complement signaling would pave the way for targeted, patient-tailored treatments in the context of precision medicine.

MATERIALS and METHODS

As mentioned in the "Data and Code Availability Statement" section, this study is a bioinformatics study in which publicly accessible data are drawn from the TCGA database. There is no need for an ethics committee, ethics and patient consent document.

Data Selection and Differential Gene Expression Analysis

The cancer genome atlas (TCGA) was used for gene expression profiling data based on RNA-seq that included more than 500 tumor and normal cases, as 500 tumor and normal cases is the smallest recommended population size for logistic regression analyses[5]. Nine different types

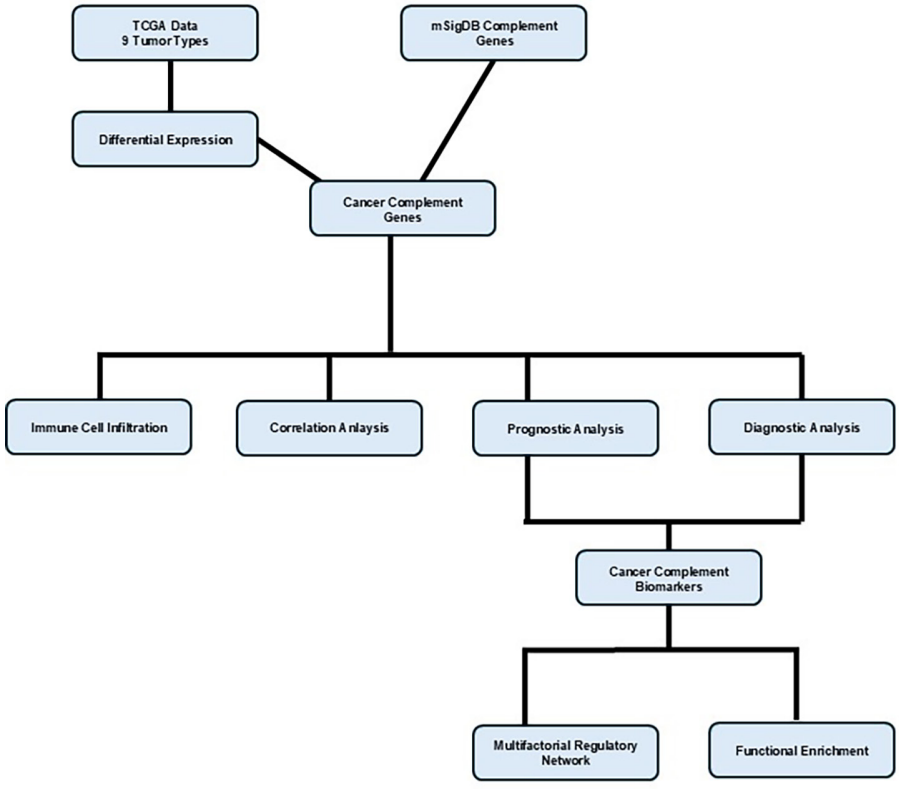

Figure 1. The study design involves several key steps. It started with acquiring gene expression datasets from the TCGA database for nine distinct cancer types. Statistical analyses were then performed on these datasets using the Bioconductor platform. Complement system-related genes were identified from the MSigDB database, and the common genes shared between the complement pathway and the nine cancers were determined. Correlation analysis was conducted to assess the similarity among tumor types. Next, immune cell infiltration levels were analyzed, and the biomarkers' prognostic and diagnostic significance were evaluated. A MRN centered on these biomarkers was then constructed, followed by pathway enrichment analysis of the regulatory elements

TCGA: The cancer genome atlas, MSigDB: Molecular signatures database, MRN: The multifactorial regulatory network

of cancer were linked to these datasets: uterine corpus endometrial carcinoma (UCEC), thyroid carcinoma (THCA), prostate adenocarcinoma (PRAD), squamous cell carcinoma of the lung (LUSC), lung adenocarcinoma (LUAD), clear renal cell carcinoma (KIRC), squamous cell carcinoma of the head and neck, adenocarcinoma of the colon (COAD), and invasive breast carcinoma (BRCA).

The R packages "TCGAbiolinks" (v.2.32.0)[6] and "DESeq2" (v.1.44.0)[7] were utilized for dataset acquisition and pre-analysis as well as differential gene expression (DEG) analysis. Logarithmic fold change (logFC) values and Benjamini-Hochberg adjusted p-values for each gene were derived from DESeq2 results. Genes that met the thresholds for logFC>1 (upregulated), logFC<-1 (downregulated), and adjusted p-value <0.05 were designated as "DEGs", following standard practices in the literature. The genes associated with the complement system were retrieved from the molecular signatures database[8].

Screening of Differential Gene Expressions Across the Complement System Associated Genes

The differentially expressed genes of each cancer type were examined for genes associated with the complement system. The DEGs of each cancer type related to the complement system were defined as "cancer complement genes" specific to that tumor type.

Similarity of Various Cancers Across the Complement System

The distance between cancer types in terms of the distribution of cancer complement genes was investigated using an analogous technique that has been used previously[9]. The simple matching coefficient (SMC) was used to calculate this distance.

$$\mathrm{SMC}\ (i, j) = \frac{\text{number of matching attribute values}}{\text{number of attributes}} = \frac{f_{00} + f_{11}}{f_{00} + f_{01} + f_{10} + f_{11}} \quad (1)$$

The SMCs were used to assess the strength of the relationships between the different cancer types, which carry cancer complement genes. Here, the two different cancer types are represented by the letters i and j; f_{00} denotes the total number of genes where neither cancer type has the matching gene in its individual cancer gene list; f_{11} denotes the total number of genes where both cancer types have the matching gene in their individual cancer gene list; And f_{10} and f_{01} represent the total number of genes where one cancer type has the matching gene in its individual cancer gene list and the other does not. The distance between the cancer types with respect to the cancer complement genes was calculated using the R package "nomclust" (v.2.8.0)[10] and visualized with the R package "corrplot" (v.0.92)[11].

Evaluation of Immune Cell Infiltration

An online portal called CIBERSORTx (https://cibersortx.stanford.edu/) was used to obtain processed data to analyse the proportion of immune cells in different types of cancer. This tool uses the *LM22* gene signature, which allows sensitive and precise identification of 22 phenotypes of human hematopoietic cells, along with a deconvolution algorithm against the gene expression data. Median gene expression values for each gene were used for each cancer type to allow comparison of cancers. For each cancer type, CIBERSORTx calculates a p-value by deconvolution. This number indicates the level of confidence in the results, and a p-value <0.05 was considered significant[12]. The number of permutations was adjusted to 1000. The distance between the cancer types in relation to the immune cell infiltration was calculated and visualized with "nomclust" and "corrplot" R packages.

Statistical Analysis

The cancer complement genes common to all types of cancers have been designated as the prospective "cancer complement biomarkers". Based on the survival data of TCGA patients, the predictive efficacy of each cancer complement biomarker was evaluated and visualized for each cancer type using the R package "Survival" (v.3.6.4)[13]. This technique allowed the classification of patients based on risk scores and prognostic performance. The p-values of the log-rank test were used to evaluate the prognostic potential of the cancer complement biomarkers.

Logistic Regression Analysis

The R package nnet (v.7.3.19)[14], was used to develop a logistic regression model that predicted associations between the cancer complement biomarkers and carcinogenesis in this study. The receiver operating characteristic (ROC) curves were generated using the "ROCR" package (v.1.0.11)[15].

Construction of a Regulatory Network

Transcription factors (TFs), microRNAs (miRNAs), and competing endogenous RNAs (ceRNAs) all influence the expression of genes. The miRNAs, that interacted with the obtained cancer complement biomarkers were predicted using mirDIP[16] and miRNet (which integrates miRNA data from 14 different miRNA databases)[17] hTFtarget miRNet (which integrates TF data from 5 different TF databases) were used to collect TF elements associated with cancer complement biomarkers[17,18]. ceRNAs that would affect

the cancer complement biomarkers were found via the Starbase[19] and LncACTdb[20] databases. The proteins in interaction with the biomarkers were obtained from BioGrid (v.4.4.235)[21].

Cytoscape (v.3.10.0) was used to map the regulatory network with protein-protein interactions[22]. The nodes of the network were determined using the "Cytohubba" plugin[23].

Functional Enrichment Analysis of Regulatory Network Elements

Gene Ontology (GO) annotation[24], *Kyoto* Encyclopedia of Genes and Genomes (KEGG) functional overrepresentation[25], Reactome functional overrepresentation[26] were all analyzed with the R package "clusterProfiler" (v.4.12.0)[27] and displayed with the R package "genekitr" (v.1.2.5)[28].

RESULTS

Transcriptome Analysis in Different Types of Cancer

Differentially expressed genes were recognized as those an adjusted p-value <0.05 and logFC >1 or logFC <-1 (Supplementary Table S1). According to the results, KIRC had the most DEGs of the nine types of cancer examined, while THCA had the fewest. All cancers except THCA had more upregulated genes than downregulated genes.

Determination of Genes of the Complement System in Different Cancer Types

A total of 522 genes potentially related to the complement system were identified (Supplementary Table S2). The DEGs of each cancer type associated with the complement system, defined as cancer complement genes specific to that tumor type, are listed in Supplementary Table S3. Supplementary Table S4 shows the binary matrix indicating the presence or absence of complement system genes in each cancer type. According to this table, all cancer types in this study showed a considerable number of cancer complement genes with differential expression. Among the 522 complement system genes, PRAD had the lowest proportion of these genes (20%), while KIRC had the highest proportion of these genes (55%).

The common elements of the complement system in different types of cancer are shown in Figure 2A. Five genes, namely apolipoprotein C1 (APOC1), component 7 (C7), complement factor-D (CFD), integrin-binding

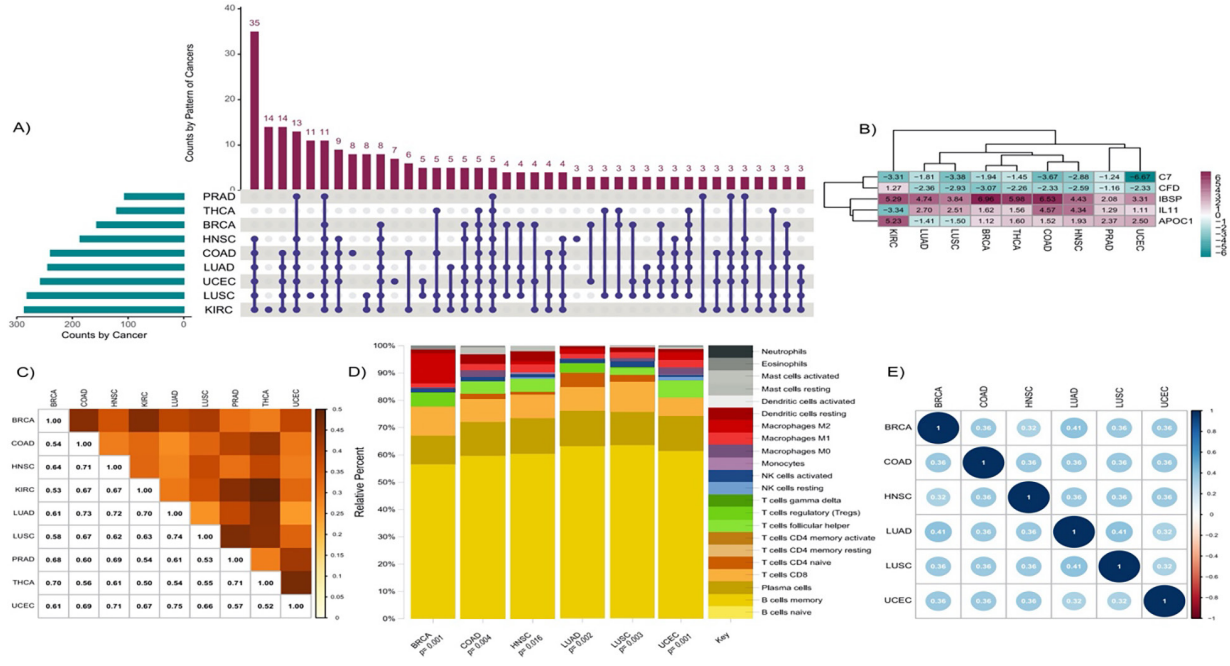

Figure 2. A) The common elements of the complement system in different types of cancer. B) The heatmap of cancer complement biomarkers. C) Simple Matching Coefficient (SMC) scores of cancer types with regard to their complement system gene composition. D) Composition of immune cells in cancers estimated by the CIBERSORTx algorithm. The bar chart shows the types of immune cells and their relative proportion in cancers. Different colors represent different cell types shown in the right bar. P<0.05 indicates significant deconvolution. E) SMC scores of cancer types with regard to their immune cell type proportion.

sialic acid protein (IBSP), and interleukin-11 (IL11), were common to all cancer types. These cancer complement genes, which are common to all cancers, were designated as the prospective "cancer complement biomarkers". The heatmap of these biomarkers expressed in all cancer types with their fold change values is shown in Figure 2B. According to this heatmap, C7 was downregulated in all cancers, and CFD was also downregulated in all cancers except KIRC. In contrast, IBSP was upregulated in all cancers, and IL11 was also upregulated in all cancers except KIRC. APOC1, on the other hand, was upregulated in all cancers except LUAD and LUSC.

Similarity Analysis Between Cancers Over the Complement System Genes

Considering the distributions of cancer complement genes, a similarity analysis was performed to calculate the distances between cancer types and to determine the strength of correlations between cancer types across these genes.

The SMC coefficients between cancers ranged from 0.50 to 0.75 (Figure 2C). The distance between THCA and KIRC was the largest (SMC=0.50), while UCEC and LUAD (SMC=0.75), and LUSC and LUAD (SMC=0.74) were the most similar cancer types in terms of cancer complement genes.

Evaluation of Immune Cell Infiltration

The immune infiltration deconvolution of each cancer was analyzed using CIBERSORTx. The results of the KIRC, PRAD, and THCA failed deconvolution (CIBERSORTx $p>0.05$), whereas the other six cancer types showed significant immune infiltrate deconvolution results (Figure 2D and Supplementary Figure S1). Of 22 immune cell types, 15 cell types were detected in two or more cancer types, while naive B-cells, gamma delta T-cells, CD4 memory resting T-cells, activated dendritic cells, CD4 memory activated T-cells, resting mast cells, and neutrophils were not detected in any of the cancer types. Memory B-cells were the most common population in six cancer types (more than 56% in all), and M2 macrophages were present at significantly higher levels in BRCA compared to the other cancer types (11%).

The SMC analysis regarding immune cells showed that LUAD and LUSC (SMC=0.41) and LUAD and BRCA (SMC=0.41) are the most strongly correlated of these six cancer types (Figure 2E).

Prognostic Potential of the Cancer Complement Biomarkers

Survival analysis was performed using the Cox regression model and Kaplan-Meier estimates, to determine the prognostic power of five potential cancer complement biomarkers for each cancer type and to emphasise the predictive power of patient survival between low and high risk groups.

Among the five biomarkers, APOC1 showed significant predictive power ($p<0.05$) for KIRC and THCA, as did C7 for LUAD, PRAD and UCEC, CFD for UCEC, IBSP for COAD, KIRC and LUAD, and IL11 for BRCA, KIRC and LUAD (Figure 3).

Diagnostic Potential of the Cancer Complement Biomarkers

A logistic regression model was developed to predict the relationship between cancers and the five prospective cancer complement biomarkers. ROC curves were generated to investigate the potential predictive value of these biomarkers in each cancer type. Figure 4 illustrates the the area under the curve (AUC) of all cancers for each biomarker.

The most common technique for determining correlations between binary outcomes and biomarkers is logistic regression, where the accuracy of a model is provided by the ROC curves. The classification scheme proposed by Hosmer and Lemeshow and confirmed in the literature for the discriminatory power of a biomarker based on the AUC is as follows: ineffective (0.0-0.5), poor (0.5-0.6), sufficient (0.6-0.7), good (0.7-0.8), very good (0.8-0.9), excellent (0.9-1.0)[29].

According to the logistic regression results, of the 45 analyses (5 biomarkers for 9 cancer types each), only 3 cases had no diagnostic significance [APOC1 for COAD (AUC=0.59), IBSP for PRAD (AUC=0.55), and IL11 for UCEC (AUC=0.29)]. The AUCs for the other cases ranged from good to excellent according to the classification of Hosmer and Lemeshow (Figure 3). To maintain figure clarity, the p-values of the Kaplan-Meier curves and the AUCs of the ROC curves are not displayed within the figures. Instead, these values are presented separately in Table 1.

Regulatory Network around Cancer Complement Biomarkers

The ceRNAs, miRNAs, TFs and proteins associated with these biomarkers are listed in Supplementary Table S5. A total of 445 elements, including 61 ceRNA, 156 miRNA, 171 TFs and 57 proteins, were found around these biomarkers. Figure 5A shows the multifactorial regulatory network (MRN) of cancer complement biomarkers. The degree and betweenness centrality analysis with the Cytohubba tool, revealed 13 elements, namely IL11, CFD, APOC1, C7, IBSP, CREB1, CTCF, EP300, MYC, P63, AR, hsa-mir-16-5p, and hsa-mir-155-5p, as hub elements (Supplementary Table S6).

Functional Enrichment Analysis

The regulatory network elements were used to investigate enriched pathways associated with the

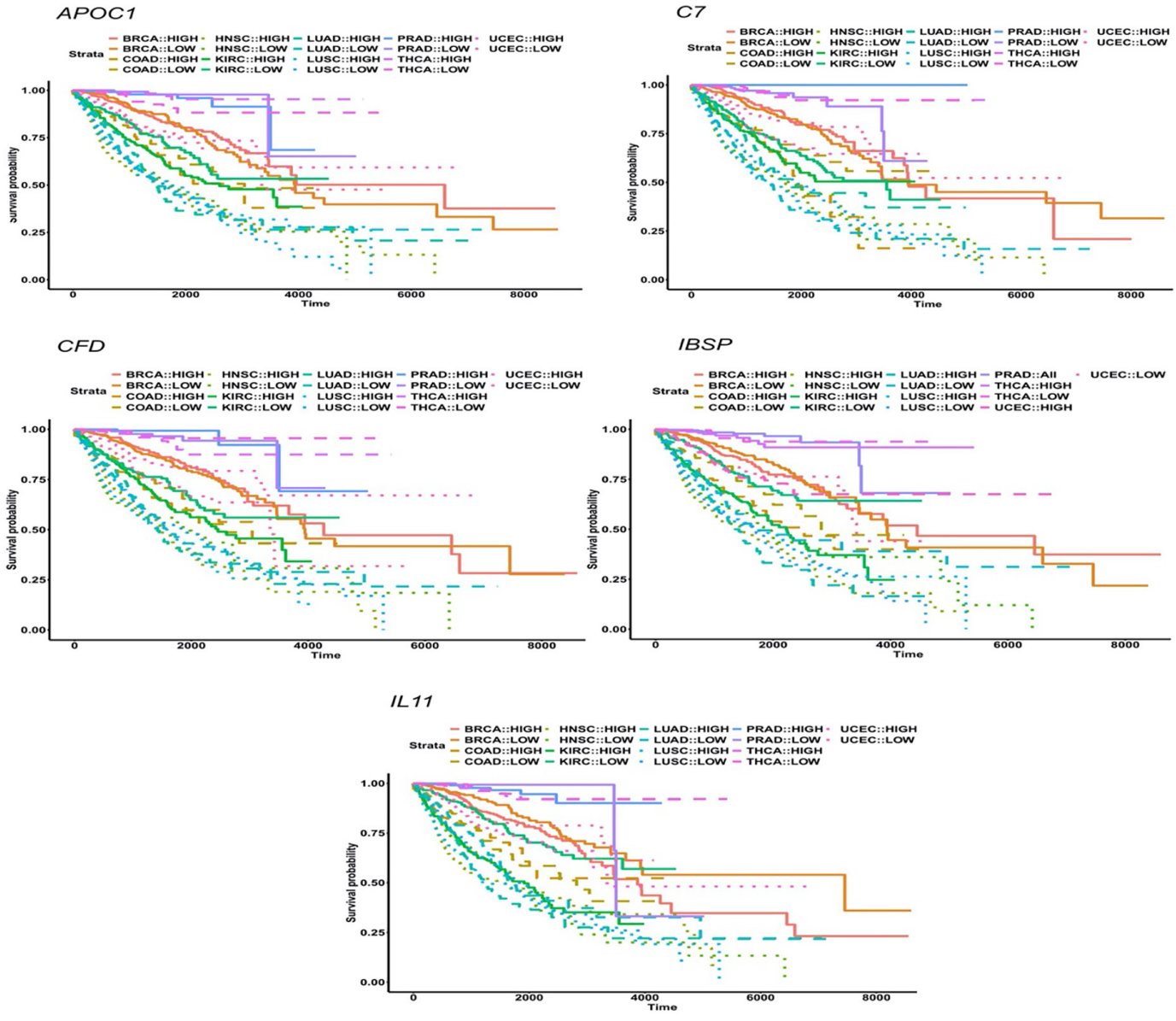

Figure 3. Kaplan-Meier plots illustrating the prognostic performance of biomarkers. A) APOC1 for all cancers. B) C7 for all cancers. C) CFD for all cancers. D) IBSP for all cancers. E) IL11 for all cancers.

APOC1: Apolipoprotein C1, C7: Component 7, CFD: Complement factor-D, IBSP: Integrin-binding sialic acid protein, IL11: Interleukin-11

Table 1. The AUCs of the diagnostic potential and the log-rank test p-values of the prognostic potential of the biomarkers for each cancer type.

	Biomarkers									
	APOC1		C7		CFD		IBSP		IL11	
Cancers	AUC	p-value	AUC	p-value	AUC	p-value	AUC	p-value	AUC	p-value
BRCA	0.76	7.6 E-01	0.85	3.8 E-01	0.92	6.4 E-01	0.97	6.4 E-01	0.79	4.9 E-02
COAD	0.59	1.9 E-01	0.97	2.3 E-01	0.98	3.8 E-01	0.9	3.8 E-02	0.93	7.8 E-01
HNSC	0.79	4.0 E-01	0.87	9.3 E-01	0.86	9.7 E-01	0.92	1.3 E-01	0.97	1.5 E-01
KIRC	0.98	3.3 E-02	0.96	2.9 E-01	0.74	7.5 E-02	0.84	1.0 E-05	0.91	4.0 E-09
LUAD	0.76	6.2 E-01	0.85	1.0 E-02	0.91	8.2 E-01	0.86	2.5 E-02	0.87	9.5 E-03
LUSC	0.91	4.7 E-01	0.98	1.3 E-01	0.99	1.2 E-01	0.91	2.9 E-01	0.85	1.1 E-01
PRAD	0.83	5.2 E-01	0.72	7.6 E-03	0.68	2.4 E-01	0.55	NA	0.79	4.5 E-01
THCA	0.74	4.7 E-02	0.83	9.7 E-01	0.93	1.2 E-01	0.89	6.8 E-01	0.72	6.5 E-01
UCEC	0.79	9.3 E-01	0.98	3.5 E-02	0.77	9.2 E-03	0.77	7.3 E-01	0.29	7.9 E-02

NA: There is only 1 group data, AUC: Area under the curve, APOC1: Apolipoprotein C1, C7: Component 7, CFD: Complement factor-D, IBSP: Integrin-binding sialic acid protein, IL11: Interleukin-11

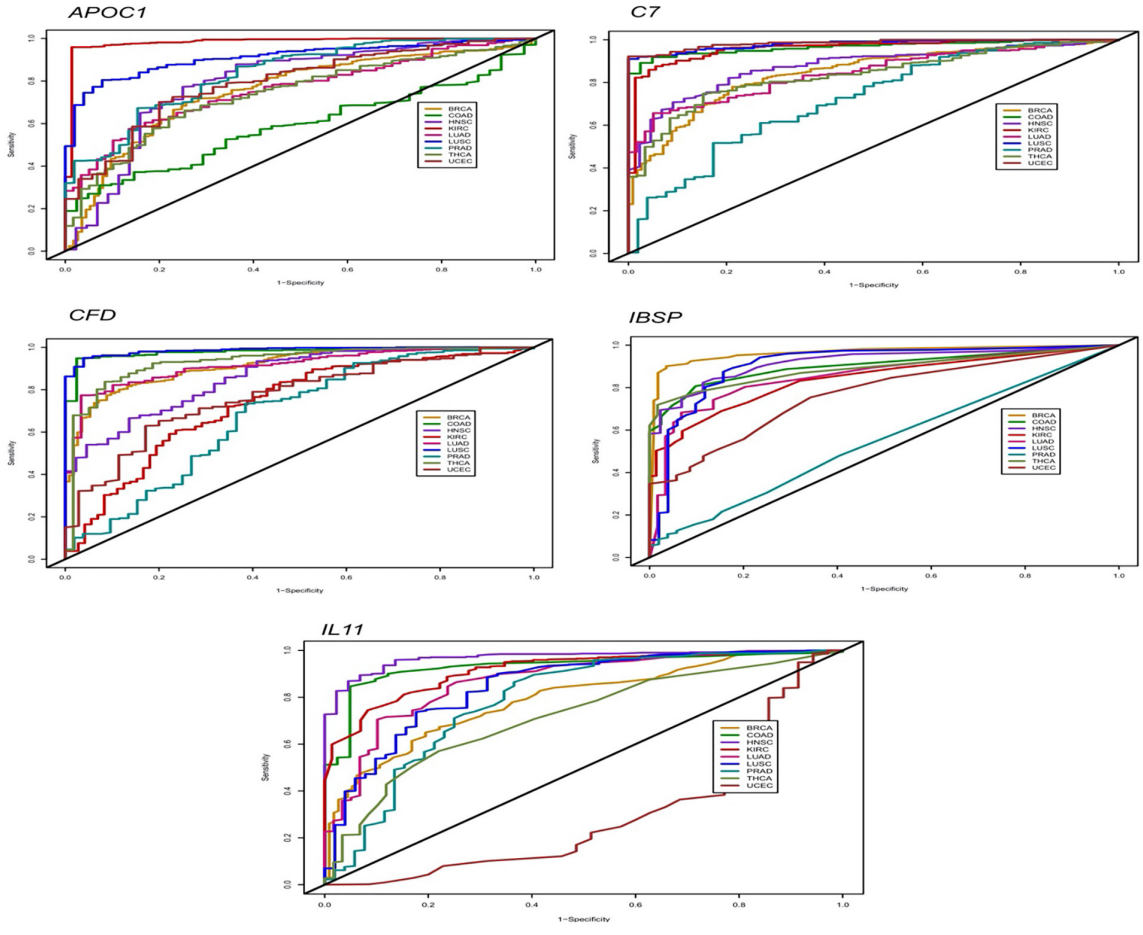

Figure 4. ROC plots displaying the diagnostic performance of biomarkers. A) APOC1 for all cancers. B) C7 for all cancers. C) CFD for all cancers. D) of IBSP for all cancers. E) IL11 for all cancers.

APOC1: Apolipoprotein C1, C7: Component 7, CFD: Complement factor-D, IBSP: Integrin-binding sialic acid protein, IL11: Interleukin-11, ROC: Receiver operating characteristic

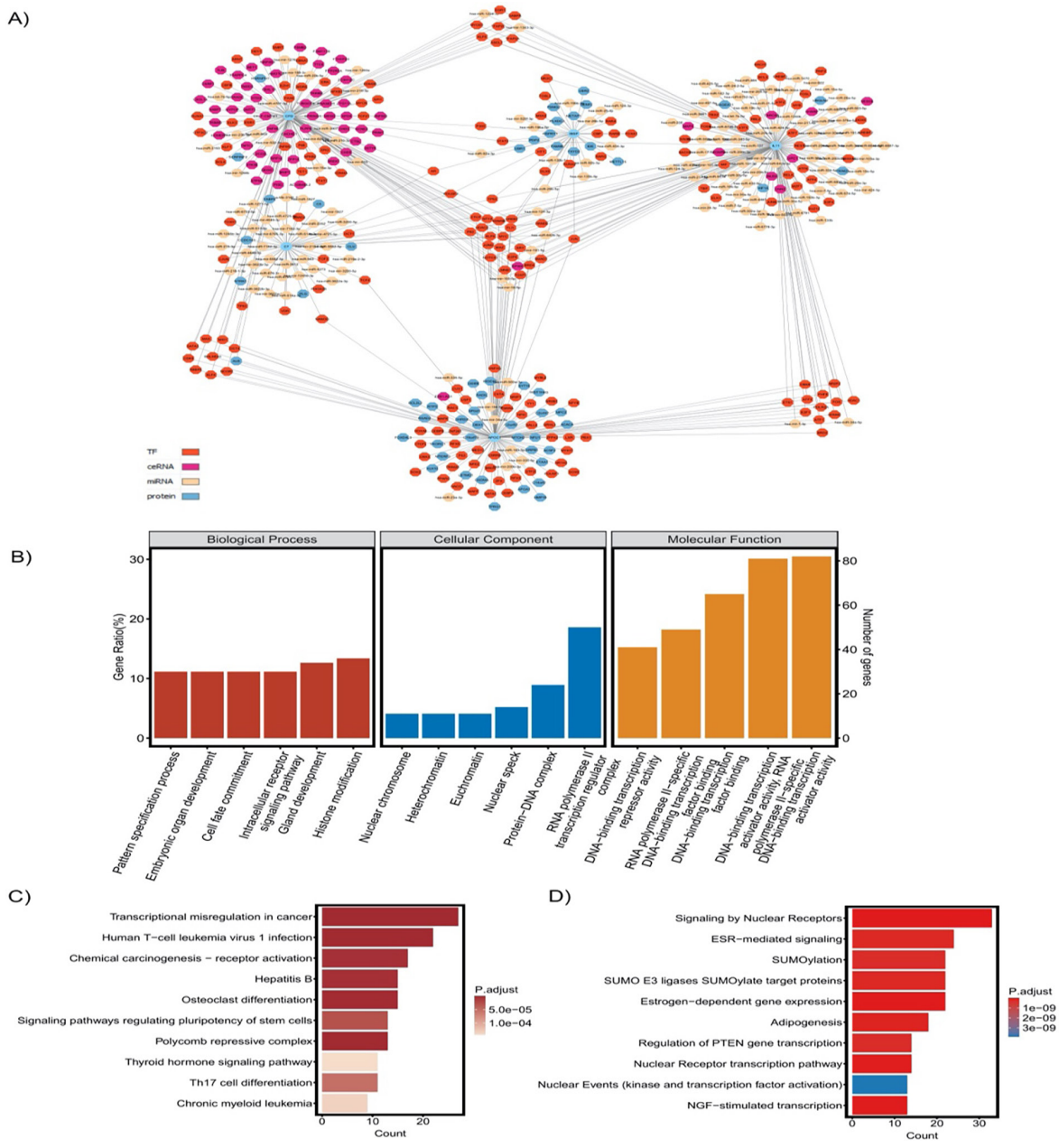

Figure 5. The multifactorial regulatory network (MRN) elements and their functional enrichment analyses. A) MRN around biomarkers and its elements. B) The wego plot of the top 10 biological processes (BPs), the top 10 cellular components (CCs) and the top 10 molecular functions (MFs). C) Kyoto Encyclopedia of Genes and Genomes overrepresentation analysis. D) Reactome overrepresentation analysis.

cancer complement biomarkers. GO annotation, KEGG functional overrepresentation, and reactome functional overrepresentation revealed that MRN elements were enriched mainly in carcinogenesis and complement system-associated pathways such as estrogen receptor signaling (ESR)-mediated signaling and SUMOylation (Figure 5B-D, Supplementary Tables S7-9).

DISCUSSION

The complement system's critical role significantly influences the development and spread of tumors, which in turn affect the prognosis and diagnosis of cancer. Researchers may be able to develop individualized treatments and gain a deeper understanding of cancer biology by using common biomarker profiles of

different cancer types within this pathway. In this work, transcriptome and clinical data from TCGA were used to identify common differentially expressed genes associated with the complement system in nine cancer types with large sample sizes.

All cancer types in this study showed a considerable number of cancer complement genes with varying levels of expression. The SMC coefficients related to cancer complement genes in different cancer types ranged from 0.50 to 0.75, suggesting that at least half of the complement system genes are shared across different cancer types. LUSC and LUAD (SMC=0.74) are among the most similar cancers in terms of cancer complement genes. Similarly, the results of CIBERSORTx show that different types of immune cells infiltrate different cancer types. As a result of the CIBERSORTx analysis, M2 macrophages were found to be significantly increased in breast cancer compared to the other cancer types, which is consistent with the study showing that M2 macrophages stimulate cell migration and growth in breast cancer[30].

The correlation between cancer types in terms of their immune cell proportions illustrates that LUAD and LUSC are the most strongly correlated of the six cancer types with significant deconvolution (SMC=0.41) (Figure 2E). These two findings are consistent with the fact that both are subtypes of lung cancer and are classified together as non-small cell lung cancer[31].

Functional enrichment analysis revealed that MRN elements were mainly enriched in pathways related to the complement system and carcinogenesis, including SUMOylation and ESR-mediated signaling. These results are consistent with the literature that SUMOylation is a post-translational modification that regulates immunological responses, carcinogenesis and DNA damage repair[32], and the ESR pathway is important in breast growth and development and is a target for breast cancer[33].

Five biomarkers, namely APOC1, C7, CFD, IBSP, and IL11, were common to all cancer types. The diagnostic and prognostic performance of these biomarkers, which were determined individually for each cancer type, shows remarkable results in most cancer types and represents an important resource for future research.

The most abundant apolipoprotein in very low density lipoprotein cholesterol is APOC. Recently, APOC1 was discovered to function as an immunological biomarker that controls macrophage polarization and contributes to the development of renal cell carcinoma[34]. This protein indicates a poor prognosis and is associated with immune infiltration of the tumor in esophageal squamous cell carcinoma[35]. The terminal component of the complement cascade, complement C7, is essential for the development of the membrane attack complex as it penetrates lipid bilayers[36]. In an omics study done by Chen et al.[37] C7 was suggested to be a novel down regulated prognostic biomarker and immunotherapy target in PRAD. This study is consistent with literature indicating that C7 was downregulated in all cancers, suggesting its tumor suppressive role (Figure 2B).

Adipsin, referred to as CFD, is a type of adipokine that is mostly produced in fat tissues and then released into the bloodstream. Also, it plays a crucial role in the activation of the complement system and serves as the rate-limiting component in the alternative complement pathway. IBSP is an essential component of bone formation, renewal and repair. Cell surface-related complexes that prevent cells from complement-mediated lysis are formed when IBSP binds to complement factor H[38]. The proliferation of cancer cells and the inflammatory microenvironment of the tumor are mediated by cytokines. Together with IL-6 and IL-27, IL-11 belongs to the family of glycoprotein 130 cytokines[39]. Numerous studies have demonstrated the possible involvement of IL-11 in a number of cancers, including prostate, ovarian, pancreatic, breast, uterine, bone, stomach, and colorectal cancers[1].

Study Limitations

This study has certain limitations. First, due to the limited availability of cancer data, the analyses were confined to TCGA, with each tumor type represented by a single dataset. While the number of cases was sufficient for statistical and logistic regression analyses, this restriction in sample size limits the generalizability of the findings. Second, transcriptome analyses primarily identify associations between diseases and traits but provide limited insight into the underlying mechanisms. Understanding how various cell types respond to therapy and impact the overall prognosis is crucial. Additionally, further research is needed to elucidate the mechanisms through which cancer complement biomarkers exert tumor-suppressive or carcinogenic effects in the examined cancer types.

CONCLUSION

In conclusion, the growth and distribution of tumors are significantly influenced by the tumor microenvironment (TME), which in turn affects the therapeutic outcome for the patient. The complement system plays an important and complex role in this scenario. It could destroy tumor cells covered with antibodies, induce localized

chronic inflammation, or suppress the T-cell response to the tumor, which promotes tumor growth. These contradictions strongly depend on the composition of the TME, the regions of complement activation, and the susceptibility of the tumor cells to the attack of the complement system, according to the latest research results. The proposed five biomarkers of this study and their surrounding network hubs open up fascinating opportunities for translational research and innovation in patient-centred healthcare and precision medicine.

Ethics

Ethics Committee Approval: This bioinformatics study utilizes publicly available data from the TCGA database. As the data are openly accessible, ethical approval and patient consent are not required.

Informed Consent: This bioinformatics study utilizes publicly available data from the TCGA database. As the data are openly accessible, ethical approval and patient consent are not required.

Footnotes

Financial Disclosure: The author declare that this study received no financial support.

REFERENCES

1. Xu DH, Zhu Z, Wakefield MR, Xiao H, Bai Q, Fang Y. The role of IL-11 in immunity and cancer. Cancer Lett. 2016;373:156-63.
2. Kolev M, Das M, Gerber M, Baver S, Deschatelets P, Markiewski MM. Inside-out of complement in cancer. Front Immunol. 2022;13:931273.
3. Roumenina LT, Daugan MV, Petitprez F, Sautès-Fridman C, Fridman WH. Context-dependent roles of complement in cancer. Nat Rev Cancer. 2019;19:698-715.
4. Özdemir V, Arga KY, Aziz RK, et al. Digging deeper into precision/personalized medicine: cracking the sugar code, the third alphabet of life, and sociomateriality of the cell. OMICS. 2020;24:62-80.
5. Bujang MA, Sa'at N, Sidik TMITAB, Joo LC. Sample size guidelines for logistic regression from observational studies with large population: emphasis on the accuracy between statistics and parameters based on real life clinical data. Malays J Med Sci. 2018;25:122-30.
6. Colaprico A, Silva TC, Olsen C, et al. TCGAbiolinks: an R/Bioconductor package for integrative analysis of TCGA data. Nucleic Acids Res. 2016;44:e71.
7. Love MI, Huber W, Anders S. Moderated estimation of fold change and dispersion for RNA-seq data with DESeq2. Genome Biol. 2014;15:550.
8. Liberzon A, Birger C, Thorvaldsdóttir H, Ghandi M, Mesirov JP, Tamayo P. The molecular signatures database (MSigDB) hallmark gene set collection. Cell Syst. 2015;1:417-25.
9. Oktem EK, Aydin B, Gulfidan G, Arga KY. A transcriptomic and reverse-engineering strategy reveals molecular signatures of arachidonic acid metabolism in 12 cancers. OMICS. 2023;27:127-38.
10. Sulc Z, Cibulkova J, Rezankova H, Hornicek J. R package nomclust: hierarchical cluster analysis of nominal data (version 2.8.0). 2023.
11. Taiyun W, Simko V. R package "corrplot": Visualization of a correlation matrix (version 0.92). 2022.
12. Newman AM, Liu CL, Green MR, et al. Robust enumeration of cell subsets from tissue expression profiles. Nat Methods. 2015;12:453-7.
13. Therneau TM, Lumley T, Atkinson E, et al. A Package for Survival Analysis in R. 2024. R package version 3.7-0. 2024.
14. Venables WN (William N), Ripley BD. Modern applied statistics with S. Vol. Fourth edition. Springer, New York; 2002. p. 495.
15. Sing T, Sander O, Beerenwinkel N, et al. ROCR: Visualizing classifier performance in R. Bioinformatics. 2005;21(20):3940–1.
16. Tokar T, Pastrello C, Rossos AEM, et al. mirDIP 4.1-integrative database of human microRNA target predictions. Nucleic Acids Res. 2018;46:D360-70.
17. Chang L, Zhou G, Soufan O, Xia J. miRNet 2.0: network-based visual analytics for miRNA functional analysis and systems biology. Nucleic Acids Res. 2020;48:W244-51.
18. Zhang Q, Liu W, Zhang HM, et al. hTFtarget: a comprehensive database for regulations of human transcription factors and their targets. Genomics Proteomics Bioinformatics. 2020;18:120-8.
19. Li JH, Liu S, Zhou H, Qu LH, Yang JH. starBase v2.0: decoding miRNA-ceRNA, miRNA-ncRNA and protein-RNA interaction networks from large-scale CLIP-Seq data. Nucleic Acids Res. 2014;42:D92-7.
20. Wang P, Guo Q, Qi Y, et al. LncACTdb 3.0: an updated database of experimentally supported ceRNA interactions and personalized networks contributing to precision medicine. Nucleic Acids Res. 2022;50:D183-9.
21. Oughtred R, Rust J, Chang C, et al. The BioGRID database: A comprehensive biomedical resource of curated protein, genetic, and chemical interactions. Protein Sci. 2021;30:187-200.
22. Shannon P, Markiel A, Ozier O, et al. Cytoscape: a software environment for integrated models of biomolecular interaction networks. Genome Res. 2003;13:2498-504.
23. Chin CH, Chen SH, Wu HH, et al. cytoHubba: identifying hub objects and sub-networks from complex interactome. BMC Syst Biol. 2014;8 Suppl 4:S11.
24. Ashburner M, Ball CA, Blake JA, et al. Gene ontology: tool for the unification of biology. The gene ontology consortium. Nat Genet. 2000;25:25-9.
25. Kanehisa M, Araki M, Goto S, et al. KEGG for linking genomes to life and the environment. Nucleic Acids Res. 2008;36:D480-4.
26. Milacic M, Beavers D, Conley P, et al. The reactome pathway knowledgebase 2024. Nucleic Acids Res. 2024;52:D672-8.
27. Yu G, Wang LG, Han Y, He QY. Clusterprofiler: an r package for comparing biological themes among gene clusters. OMICS. 2012;16:284-7.
28. Liu Y, Li G. Empowering biologists to decode omics data: the genekitr r package and web server. BMC Bioinformatics. 2023;24:214.
29. Maranhão BHF, da Silva Junior CT, Barillo JL, et al. Diagnostic accuracy with total adenosine deaminase as a biomarker for discriminating pleural transudates and exudates in a population-based cohort study. Dis Markers. 2021;2021:6648535.

30. Tu D, Dou J, Wang M, Zhuang H, Zhang X. M2 macrophages contribute to cell proliferation and migration of breast cancer. Cell Biol Int. 2021;45:831-8.

31. Chen JW, Dhahbi J. Lung adenocarcinoma and lung squamous cell carcinoma cancer classification, biomarker identification, and gene expression analysis using overlapping feature selection methods. Sci Rep. 2021;11:13323.

32. Han ZJ, Feng YH, Gu BH, Li YM, Chen H. The post-translational modification, SUMOylation, and cancer (Review). Int J Oncol. 2018;52:1081-94.

33. Kumar D, Myers M, Al Homsi U, Ilyin, V. Role of ESR pathway genes in breast cancer: a review. Adv Breast Cancer Res. 2018;7:134-86.

34. Ren L, Yi J, Yang Y, et al. Systematic pan-cancer analysis identifies APOC1 as an immunological biomarker which regulates macrophage polarization and promotes tumor metastasis. Pharmacol Res. 2022;183:106376.

35. Cao X, Wu B, Guo S, et al. APOC1 predicts a worse prognosis for esophageal squamous cell carcinoma and is associated with tumor immune infiltration during tumorigenesis. Pathol Oncol Res. 2023;29:1610976.

36. Würzner R. Modulation of complement membrane attack by local C7 synthesis. Clin Exp Immunol. 2000;121:8-10.

37. Chen Z, Yan X, Du GW, et al. Complement C7 (C7), a potential tumor suppressor, is an immune-related prognostic biomarker in prostate cancer (PC). Front Oncol. 2020;10:1532.

38. Pan B, Cheng X, Tan W, et al. Pan-cancer analysis shows that IBSP is a potential prognostic and immunotherapeutic biomarker for multiple cancer types including osteosarcoma. Front Immunol. 2023;14:1188256.

39. Kishimoto T, Akira S, Narazaki M, Taga T. Interleukin-6 family of cytokines and gp130. Blood. 1995;86:1243-54.

Supplementary Figure 1: https://l24.im/QBuFUx

Supplementary Table 1: https://l24.im/hf5zM

Supplementary Table 2: https://l24.im/VB4sZm

Supplementary Table 3: https://l24.im/aKS0tH

Supplementary Table 4: https://l24.im/Wenk

Supplementary Table 5: https://l24.im/49qWiFJ

Supplementary Table 6: https://l24.im/ELC9U

Supplementary Table 7: https://l24.im/kOLqPK

Supplementary Table 8: https://l24.im/dLTx

Supplementary Table 9: https://l24.im/C9mzsQ

DOI: 10.4274/MMJ.galenos.2024.47042
Medeni Med J 2025;40:12-17

Original Article

The Lateral Femoral Cutaneous Nerve is at High Risk During Direct Anterior Approach to the Hip Joint Due to Proximity and Anatomic Variations: A Cadaveric Study

Lateral Femoral Kutanöz Sinir, Yakınlık ve Anatomik Varyasyonlardan Dolayı Kalça Eklemine Direkt Anterior Yaklaşım Sırasında Yüksek Risk Altındadır: Bir Kadavra Çalışması

Dang Hoang GIANG[1], Thanh Xuan DAO[1], Du Gia HOANG[2]

[1]Hanoi Medical University Faculty of Medicine, Department of Surgical, Hanoi, Vietnam
[2]Bach Mai Hospital, Clinic of Orthopedic Trauma, Hanoi, Vietnam

ABSTRACT

Objective: In direct anterior approach (DAA) to the hip joint, the risk of lateral femoral cutaneous nerve (LFCN) injury is high. This study on cadavers aimed to identify variations in the anatomy and route of the LFCN and its relationship with the DAA.

Methods: The cross-sectional study was conducted on 15 adult formalin-embalmed cadavers [8 males and 7 female (15 paired hips)]. The anterior superior iliac spine, pubic tubercle, and fibular head were used as anatomical reference points.

Results: All 30 portals were inserted completely without damage or complications at the anatomical sites. The mean age standard deviation was 72.0 (16.8) range: 26-91 years old. Nineteen nerves crossed the incision. The branching pattern of the lateral cutaneous nerve of the thigh below the inguinal ligament is predominantly fan type (12 nerves, 40.0%), followed by sartorius type (11 nerves, 37.0%), with a lower percentage being posterior type (7 nerves, 23.3%). The average distance from the initial point to the location where the lateral cutaneous nerve of the thigh crosses the surgical incision was 35.3 (16.4-62.9) mm, with a range of 2.3-92.2 mm.

Conclusions: The risk of LFCN injury was 50%. Understanding variations in the anatomy and route of the LFCN and its proximity to the incision of the DAA to the hip joint may reduce the risk of injury.

Keywords: LFCN, DAA, injury, lateral femoral cutaneous nerve, direct anterior approach

ÖZ

Amaç: Kalça eklemine doğrudan anterior yaklaşımda (DAA), lateral femoral kutanöz sinir (LFCN) yaralanması riski yüksektir. Kadavralar üzerinde yapılan bu çalışma, LFCN'nin anatomisi ve rotasındaki varyasyonları ve DAA ile ilişkisini belirlemeyi amaçlamıştır.

Yöntemler: Bu kesitsel çalışma 15 erişkin formalinle mumyalanmış kadavra [8 erkek ve 7 kadın (15 çift kalça)] üzerinde yürütüldü. Anatomik referans noktaları olarak anterior superior iliyak diken, pubik tüberkül ve fibula başı kullanıldı.

Bulgular: Tüm 30 portal, anatomik bölgelerde hasar veya komplikasyon olmadan tamamen yerleştirildi. Ortalama yaş standart sapma 72,0 (16,8) idi (aralık: 26-91). On dokuz sinir kesiyi geçti. Uyluğun lateral kutanöz sinirinin inguinal ligamentin altında dallanma deseni baskın olarak fan tipidir (12 sinir, %40,0), bunu sartorius tipi (11 sinir, %37,0) takip eder ve daha düşük bir yüzde posterior tiptir (7 sinir, %23,3). Uyluğun lateral kutanöz sinirinin cerrahi kesiyi geçtiği yere başlangıç noktasından ortalama uzaklık 35,3 (16,4-62,9) mm, aralık ise 2,3-92,2 mm'dir.

Sonuçlar: LFCN yaralanma riski %50 idi. LFCN'nin anatomisindeki ve rotasındaki varyasyonları ve kalça eklemine DAA kesisine yakınlığını anlamak yaralanma riskini azaltabilir.

Anahtar kelimeler: LFCN, DAA, yaralanma, lateral femoral kutanöz sinir, direkt anterior yaklaşım

Address for Correspondence: T. X Dao, Hanoi Medical University Faculty of Medicine, Department of Surgical, Hanoi, Vietnam
E-mail: daoxuanthanh@hmu.edu.vn **ORCID ID:** orcid.org/0000-0002-2245-8202

Cite as: Giang DH, Dao TX, Hoang DG. The lateral femoral cutaneous nerve is at high risk during direct anterior approach to the hip joint due to proximity and anatomic variations: a cadaveric study. Medeni Med J. 2025;40:12-17

Received: 23 September 2024
Accepted: 23 December 2024
Epub: 5 February 2025
Published: 28 March 2025

INTRODUCTION

The direct anterior approach (DAA) for uncemented and cemented total hip arthroplasty, which involves a minimally invasive incision between the sartorius and tensor fascia latae muscles, has become increasingly beneficial for surgeons. It offers easier access to the hip joint, reduces intraoperative blood loss, and enhances control over the positioning of artificial joint components and leg length alignment[1,2]. Additionally, this technique helps lower the risk of postoperative complications, such as dislocation, leg length discrepancy, and sciatic nerve injury[1-3].

Although it resolves many shortcomings of the posterior approach, the standard DAA presents a significant risk of damaging the lateral femoral cutaneous nerve (LFCN), causing sensory issues in the anterolateral thigh and impacting the patient's postoperative quality of life[4,5]. Several applied anatomical studies have aimed to identify the ideal incision location for the DAA to prevent LFCN injury while maintaining easy access to the hip joint. This technique involves making a skin incision 2 cm below and lateral to the anterior superior iliac spine (ASIS), just above the belly of the tensor fasciae latae muscle[6,7].

Thus, this study aimed to describe the route of the LFCN and its proximity to the DAA for Vietnamese patients.

MATERIALS and METHODS

The study was conducted on 15 adult formalin-embalmed cadavers: 8 male and 7 female (15 paired hips). All the included adults were 18 years of age or older. The mean age (SD) was 72.0 (16.8) range 26-91 years old. The exclusion criteria consist of signs of trauma, tumors, congenital malformations, and previous surgeries around the hip joint that changed the anatomical structures in the pelvic and groin areas.

After obtaining the necessary research samples, we prepared protective gear, dissection instruments, anatomical markers, and an electronic Palmer caliper with a precision of 0.01 mm (ABSOLUTE Mitutoyo Series 500 digital caliper). The dissection was performed using the ASIS, pubic tubercle, and fibular head as anatomical reference points[2]. A 10 cm direct anterior incision was made starting below the ASIS. The incision was made 2 cm distal and 2 cm lateral from the ASIS, running parallel to the line between the ASIS and fibular head. The LFCN and its branches were dissected at the level of the inguinal ligament, along with related structures in the thigh area, comprising the inguinal ligament, the lateral border of the sartorius muscle, and the medial border of the tensor fasciae latae muscle.

The anatomical landmarks are identified as follows:

A: Center of the ASIS (Figure 1a-c).

B: The location where the lateral cutaneous nerve of the thigh crosses the inguinal ligament. If two branches existed, they were numbered sequentially from lateral to medial, such as B1, B2 (Figure 1a-c).

DD': Beginning and end points of direct anterior surgical incision (Figure 1a-c).

D1: A point along the surgical line DD' used to measure the shortest distance to the lateral cutaneous nerve of the thigh (Figure 1a-c).

C: Point at which the lateral cutaneous nerve of the thigh intersects the surgical line DD'. If multiple nerve branches intersect, label them as C1, C2, C3, etc. (Figure 1a-c).

Measurement Details:

The nerve's anatomical variations and branching patterns were documented.

The distance was measured from the midpoint of the ASIS to the LFCN where it ran across the inguinal ligament level (AB; Figure 1a-c).

If the lateral cutaneous nerve of the thigh intersects the surgical incision, the distance was measured from the start of the incision to the point where the nerve crossed the incision (DC, D'C; Figure 1a-c).

If the LFCN does not cross the incision, the shortest distance is measured from the incision line DD' to the LFCN incision line (DD'tk; Figure 1a-c).

Regarding the branching patterns of the LFCN below the inguinal ligament, we used Rudin's classification based on the size of the nerve branches, as well as the position of the branches relative to the lateral edge of the sartorius muscle and the medial edge of the tensor fascia latae muscle[5].

Statistical Analysis

The data were analyzed using SPSS version 22.0. Categorical variables are presented as counts and percentages, whereas quantitative variables are presented as mean ± standard deviation (SD) or median (interquartile range), based on whether the data follow a normal distribution. Differences between independent groups were assessed using the chi-square test and t-test or analysis of variance.

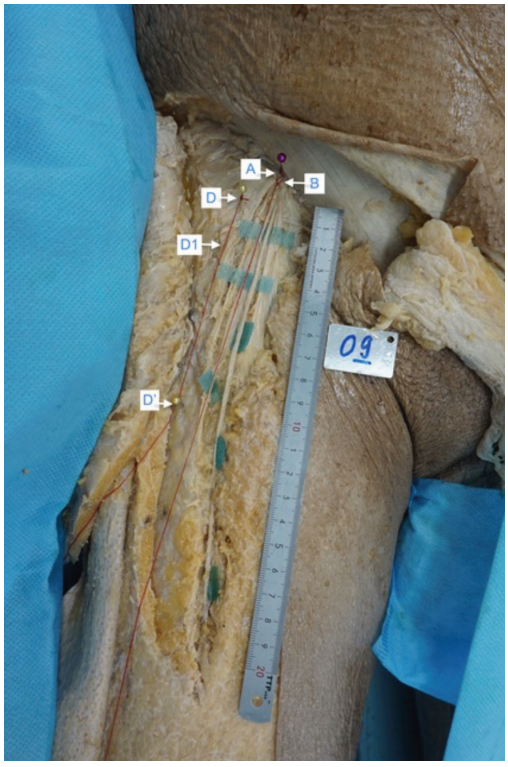

Figure 1a. Posterior type branch.

Figure 1b. Sartorius-type branch.

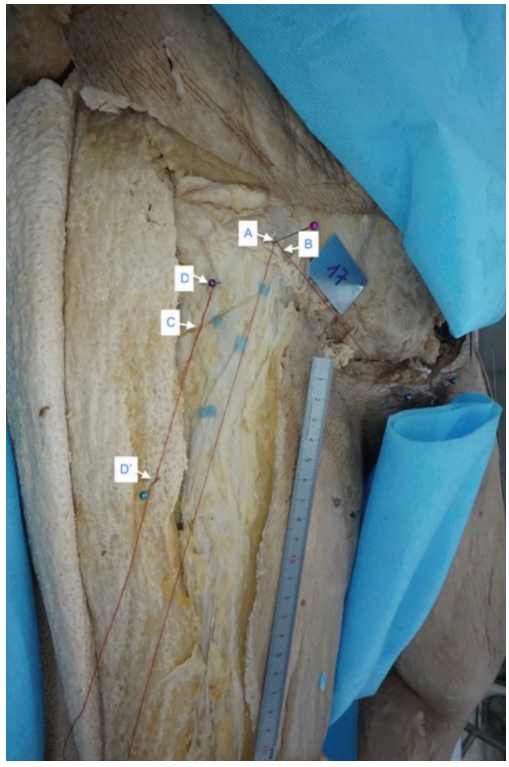

Figure 1c. Fan-type branch.

Ethical Committee Information

The study was conducted in accordance with the Declaration of Helsinki and was approved by the Ethics Committee of Hanoi Medical University in Hanoi, Vietnam (reference number: 885/GCN-HDDDNCYSH-DHYHN, date: 27.03.2023).

Informed Consent: All local and international ethical guidelines and laws pertaining to the use of human cadaveric donors in anatomical research were followed.

RESULTS

Data from all 30 specimens were collected. No damage or complications occurred at the anatomical sites. Of the total of 30 hips, 63.3% showed intersection through the surgical incision, including 3 branching patterns in the lateral cutaneous nerve of the thigh (Figure 2). The branching pattern of the lateral cutaneous nerve of the thigh below the inguinal ligament was predominantly fan type (12 nerves, 40.0%), followed by sartorius type (11 nerves, 37.0%) and posterior type (7 nerves, 23.3%).

The lateral cutaneous nerve of the thigh can branch in 3 ways: as a posterior-type branch, a sartorius-type branch, or a fan-type branch (Figure 1a-c).

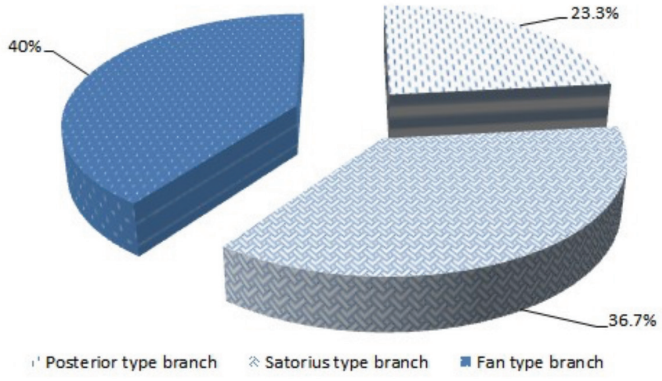

Figure 2. Prevalence of branching patterns in the LFCN below the inguinal ligament (n=30).

LFCN: Lateral femoral cutaneous nerve

Table 1 shows the thigh area origin characteristics and mean distance from the ASIS to the LFCN.

Most of the lateral cutaneous nerves of the thigh intersecting the surgical incision belonged to the fan-type group (66.7%), followed by posterior-type branches (26.7%), with only one case being the sartorius type (Table 2).

The mean distance from the initial point to the location where the lateral cutaneous nerve of the thigh crossed the surgical incision was 35.3 (16.4-62.9) mm, with a range of 2.3-92.2 mm (Table 3).

Table 4 presents the differences in mean distances of LFCN to ASIS along the inguinal ligament between male and female. However, there was no statistically significant difference in this relation.

Table 1. Features of the thigh's lateral cutaneous nerve at the inguinal ligament location (n=30).

Features	**n (%)**
Characteristics of patients entering the thigh region, n (%)	
Below the anterior superior iliac spine	15 (50.0)
Through the anterior superior iliac spine	13 (43.3)
Upper superior iliac spine	2 (6.7)
Distance from the anterior superior iliac spine to the LFCN (mm)	**Mean ± SD**
Mean ± SD	18.6±15.2
Median (IQR), min-max	12.5 (8.4-22.3), 5.5-54.3

LFCN: Lateral femoral cutaneous nerve, IQR: Interquartile range, SD: Standard deviation, IQR: Interquartile range

DISCUSSION

In the 30 cadavers dissected, we found only 2 nerves exiting the pelvis lateral to the ASIS, whereas 28 (93.3%) entered the thigh at the ASIS (of which 15 were directly below the ASIS and 13 were through the ASIS). Regarding the distance from the ASIS to the nerve, we recorded 2 cases (cadavers number 21 and 25) in which the nerve entered the thigh lateral to the ASIS. The distances from the ASIS were 49.9 mm and 7.7 mm, respectively.

According to this classification, the fan- and sartorius-type patterns accounted for the majority, accounting for 77% (40.0% and 37.0%, respectively). The posterior type pattern was the least common (23.3%).

Our results are consistent with the cadaver dissection studies conducted by Thaler (2020, n=44), and Phruetthiphat (2021, n=30). However, all authors observed a higher prevalence of the sartorius type pattern, with proportions of 60% (Phruetthiphat), and 70.5% (Thaler), whereas, in our study, the sartorius type pattern was found in only 37% of cases[6,7]. The difference may be due to variations in the assessment of the nerve branch sizes and the morphology of the two groups because both branches run anteriorly along the lateral border of the sartorius muscle, making it difficult to distinguish between the two patterns[8,9]. This challenge was also reported by Sugano et al.[10] (n=64) during the dissection of 64 lateral cutaneous nerves of the thigh,

Table 2. Features of the lateral cutaneous nerve of the thigh that intersect the direct anterior surgical incision.

Features	**n (%)**
Large and small branches	
Large branch	3 (20.0)
Small branch	11 (73.3)
Both	1 (6.7)
Amount of cutting branches	
1 branch	2 (13.3)
2 branches	5 (33.3)
3 branches	7 (46.7)
4 branches	1 (6.7)
Branching patterns	
Posterior type	4 (26.6)
Sartorius type	1 (6.7)
Fan type	10 (66.7)
Cutting position	
1/3 above	7 (46.7)
1/3 middle	4 (26.7)
1/3 under	4 (26.7)

where the author suggested combining the sartorius and fan-shaped patterns into a single anterior branch pattern (63%). This pattern closely corresponds with our findings when combining the sartorius and fan type groups[10].

The fan-type pattern was most frequently intersected by the DAA (10 nerves, 66.7%), followed by the posterior type branch and fan-type branch with 4 nerves (26.7%) and 1 nerve (6.7%) respectively, with 10 out of 12 (82.3%) fan-type lateral cutaneous nerves of the thigh being cut. Our findings are consistent with those of many other studies, which also suggest that because of the numerous small branches innervating the entire anterolateral thigh, intersection by the DAA is unavoidable[5,6,10].

A study in Japan, considered the largest dissection study with 64 cadavers, conducted by Sugano et al.[10], reported that the DAA intersected 42% of the posterior type branch, which is similar to our result of 4 out of 7 (57.1%). However, the anterior branch patterns (sartorius and fan-type) did not intersect in any of the patients. This discrepancy may be due to differences in the classification of the LFCN into branches.

In the 15 lateral cutaneous nerves of the thigh not intersected by the DAA, the sartorius branch was the most common, accounting for 10 out of 15 (66.7%), followed by the posterior type branch with 3 out of 15 (20.0%) and 2 out of 15 (13.3%) for the other branches. Most of the sartorius-type branches did not intersect, with 10 out of 11 (90.9%) remaining intact. These results are consistent with the findings of most previous studies[6,7]. According to the data from our measurements, starting the incision 3 cm distal and 4 cm posterior to the ASIS and extending the incision toward the fibular head decreased the risk of LFCN injury by 20%.

Table 3. Distance from the initial point to the location where the lateral cutaneous nerve of the thigh crosses the surgical incision.

Distance (mm)	Mean±SD	Min.-max.
DC1 (n=15)	19.9±13.7	2.3-49.5
DC2 (n=13)	43.3±22.4	5.8-80.7
DC3 (n=8)	70.0±22.0	18.9-92.9
DC4 (n=1)	38.6	-
Median DC (IQR)	35.3 (16.4-62.9)	2.3-92.2

IQR: Interquartile range, Min.-max.: Minimum-maximum, SD: Standard deviation

Table 4. Mean distances between LFCN and ASIS along the inguinal ligament.

Gender	Side	Mean distance (mm)	Standard deviation	Min-max	p-value
Female	Left	21.1	22.0	5.5-46.3	0.98
	Right	21.5	14.6	10.4-38.0	
Male	Left	21.2	19.5	6.7-54.3	0.65
	Right	14.4	7.1	8.4-22.3	

LFCN: Lateral femoral cutaneous nerve, ASIS: Anterior superior iliac spine

The closest distance from the incision to the nerve is 9.9±5.8 mm, with this position being on average 41.4±36 mm from the starting point of the incision. The nerve was very close to the incision, particularly within the upper and middle thirds of the incision. Therefore, during dissection, it is important to thoroughly separate the deep fatty layers and to avoid placing retractor instruments in these areas to prevent nerve compression throughout the surgical procedure[3,11].

Study Limitations

The research was conducted after the end of the coronavirus disease-2019 pandemic period, and we encountered significant difficulties with administrative processes and in selecting suitable cadavers for the study. Additionally, because the study involved cadaver dissection, we could not assess factors related to treatment outcomes or the demographic characteristics of patients. At cadaver insertion, we did not measure the weight or height.

CONCLUSION

The anatomical features of the LFCN were mainly the fan-shaped and sartorius types. Understanding the distance between the nerve and direct anterior incision can help surgeons reduce the risk of complications during total hip arthroplasty.

Ethics

Ethics Committee Approval: The study was conducted in accordance with the Declaration of Helsinki and was approved by the Ethics Committee of Hanoi Medical University in Hanoi, Vietnam (reference number: 885/GCN-HDDDNCYSH-DHYHN, date: 27.03.2023).

Informed Consent: All local and international ethical guidelines and laws pertaining to the use of human cadaveric donors in anatomical research were followed.

Footnotes

Author Contributions

Surgical and Medical Practices: D.H.G., T.X.D., D.G.H., Concept: D.H.G., T.X.D., D.G.H., Design: D.H.G., T.X.D.,

D.G.H., Data Collection and/or Processing: D.H.G., T.X.D., D.G.H., Analysis and/or Interpretation: D.H.G., T.X.D., D.G.H., Literature Search: D.H.G., T.X.D., D.G.H., Writing: D.H.G., T.X.D., D.G.H.

Conflict of Interest: The authors have no conflict of interest to declare.

Financial Disclosure: The authors declared that this study has received no financial support.

REFERENCES

1. Haynes JA, Hopper RH Jr, Ho H, et al. Direct anterior approach for primary total hip arthroplasty lowers the risk of dislocation compared to the posterior approach: a single institution experience. J Arthroplasty. 2022;37:495-500.
2. Curtin BM, Edwards PK, Odum S, et al. Anterior capsulectomy versus repair in direct anterior total hip arthroplasty. Eur J Orthop Surg Traumatol. 2023;33:3649-54.
3. Mangla N, Wadhwa S, Mishra S, et al. Cadaveric study of variations in the course of lateral femoral cutaneous nerve: insight to prevent injury. Medeni Med J. 2023;38:172-9.
4. Dahm F, Aichmair A, Dominkus M, et al. Incidence of lateral femoral cutaneous nerve lesions after direct anterior approach primary total hip arthroplasty - a literature review. Orthop Traumatol Surg Res. 2021;107:102956.
5. Rudin D, Manestar M, Ullrich O, et al. The anatomical course of the lateral femoral cutaneous nerve with special attention to the anterior approach to the hip joint. J Bone Joint Surg Am. 2016;98:561-7.
6. Phruetthiphat OA, Sangthumprateep V, Trakulngernthai S, et al. Functional outcome and complication following THA through modified direct anterior approach correlated to cadaveric study: are there any differences in Asian hip? J Orthop Surg Res. 2021;16:513.
7. Thaler M, Dammerer D, Hechenberger F, et al. The anatomical course of the lateral femoral cutaneous nerve in relation to various skin incisions used for primary and revision total hip arthroplasty with the direct anterior approach. J Arthroplasty. 2021;36:368-73.
8. Grothaus MC, Holt M, Mekhail AO, et al. Lateral femoral cutaneous nerve: an anatomic study. Clin Orthop Relat Res. 2005;437:164-8.
9. Ukai T, Suyama K, Hayashi S, et al. The anatomical features of the lateral femoral cutaneous nerve with total hip arthroplasty: a comparative study of direct anterior and anterolateral supine approaches. BMC Musculoskelet Disord. 2022;23:267.
10. Sugano M, Nakamura J, Hagiwara S, et al. Anatomical course of the lateral femoral cutaneous nerve with special reference to the direct anterior approach to total hip arthroplasty. Mod Rheumatol. 2020;30:752-7.
11. Sariali E, Leonard P, Mamoudy P. Dislocation after total hip arthroplasty using Hueter anterior approach. J Arthroplasty. 2008;23:266-72.

DOI: 10.4274/MMJ.galenos.2025.22725
Medeni Med J 2025;40:18-25

Original Article

Protective Effect of Boric Acid on Oxidative Damage and Cognitive Function in Aging Modeled Rats

Yaşlı Sıçan Modelinde Borik Asidin Oksidatif Hasar ve Bilişsel Fonksiyonlar Üzerine Koruyucu Etkisi

Emel SERDAROGLU KASIKCI[1], Burcu CEVRELI[2], Feride Nihal SINAN[3], Zeynep GURDERE[1], Aylin SONMEZ[1], Rumeysa SONMEZ[1]

[1]Uskudar University Faculty of Engineering and Natural Sciences, Department of Molecular Biology and Genetics, Istanbul, Türkiye
[2]Uskudar University Faculty of Medicine, Department of Physiology, Istanbul, Türkiye
[3]Uskudar University Graduate School of Science, Department of Biotechnology, Istanbul, Türkiye

ABSTRACT

Objective: Aging is a degenerative process. Therefore, the background of our study is to evaluate the effects of boron, one of the important underground resources in Türkiye, on aging and related diseases. This study aimed to assess the antioxidant effect and the cognitive functions of boric acid (BA) in a D-galactose (D-gal)-induced aging model.

Methods: Eight male Wistar rats, each 12 weeks old, were split into four groups at random: control, D-gal, BA and D-gal+BA. An experimental aging model was induced by a single subcutaneous injection of D-gal (150 mg/kg/day), and BA (100 mg/kg/day) was administered by oral gavage for 12 weeks. The novel object recognition test (NORT) and Morris water maze (MWM) were used to evaluate the cognitive ability of rats.

Results: At the end of the experimental period, glutathione (GSH) and malondialdehyde (MDA) levels were assessed in serum and brain tissue. The treatment of D-gal induced aging rats with BA significantly decreased the MDA level ($p<0.05$) and increased the GSH level, although the increase was not significant. Moreover, NORT and MWM tests showed that BA significantly improved ($p<0.05$) cognitive deficits in D-Gal + BA treated rats.

Conclusions: BA prevents D-gal-induced memory deficit by decreasing oxidative stress. Hence, BA was a good candidate for addressing age-related neurodegenerative disorders and cognitive function improvements.

Keywords: Boric acid, D-galactose, aging, oxidative stress, rat

ÖZ

Amaç: Yaşlanma dejeneratif bir süreçtir. Bu nedenle çalışmamızın arka planı, Türkiye'nin önemli yeraltı kaynaklarından biri olan borun yaşlanma ve ilişkili hastalıklar üzerindeki etkilerini değerlendirmektir. Bu çalışma, D-galaktoz (D-gal) kaynaklı yaşlanma modelinde borik asidin (BA) antioksidan etkisini ve bilişsel işlevlerini değerlendirmeyi amaçlamaktadır.

Yöntemler: On iki haftalık erkek Wistar sıçanlar (n=8) rastgele dört gruba ayrıldı; kontrol, D-gal, BA ve D-gal+BA. Deneysel yaşlanma modeli, 12 hafta boyunca D-gal (150 mg/kg/gün) tek doz deri altı enjeksiyonu ve BA (100 mg/kg/gün) oral gavaj uygulanarak oluşturuldu. Sıçanların bilişsel yeteneklerini değerlendirmek için yeni nesne tanıma testi (NORT) ve Morris su labirenti (MWM) testi kullanıldı.

Bulgular: Deneysel periyodun sonunda, serum ve beyin dokusunda glutatyon (GSH) ve malondialdehit (MDA) seviyeleri değerlendirildi. D-gal ile uyarılan yaşlı sıçanların BA ile tedavisi MDA seviyesini anlamlı ölçüde azalttı ($p<0,05$), ancak GSH seviyesini önemli ölçüde artırmadı. Üstelik, NORT ve MWM testleri, BA'nın D-gal +BA ile tedavi edilen sıçanlarda bilişsel eksikliği önemli ölçüde iyileştirdiğini gösterdi ($p<0,05$).

Sonuçlar: Sonuç olarak, BA oksidatif stresi azaltarak D-gal ile uyarılan hafıza eksikliğini önlemektedir. Bu nedenle, BA yaşa bağlı nörodejeneratif bozukluklar ve bilişsel işlevler için iyi bir adaydır.

Anahtar kelimeler: Borik asit, D-galaktoz, yaşlanma, oksidatif stres, sıçan

INTRODUCTION

Aging is a degenerative process that raises the risk of illness and mortality while also causing a time-dependent deterioration in physiological functions. According to studies, the number of functionally competent mitochondria in post-mitotic cells may decrease with age due to progressive membrane damage caused by free radicals and lipid peroxides, which are by-products of oxygen reduction during respiration. Additionally, cellular adenosine triphosphate production may decrease and peroxide production may increase as a result of this

Address for Correspondence: B. Cevreli, Üsküdar University Faculty of Medicine, Department of Physiology, Istanbul, Türkiye
E-mail: burcu.cevreli@uskudar.edu.tr **ORCID ID:** orcid.org/0000-0001-6337-4999

Cite as: Serdaroglu Kasikci E, Cevreli B, Sinan FN, Gurdere Z, Sonmez Z, Sonmez R. Protective effect of boric acid on oxidative damage and cognitive function in aging modeled rats. Medeni Med J. 2025;40:18-25

Received: 11 November 2024
Accepted: 27 February 2025
Epub: 14 March 2025
Published: 28 March 2025

damage[1]. The majority of intracellular reactive oxygen species (ROS) are assumed to be generated as a byproduct of the respiratory chain's oxidation-reduction processes in the mitochondria[2]. ROS's principal intracellular source is the mitochondria, which can be directly attacked by generated ROS[3]. However, it is widely acknowledged that ROS overproduction and leakage from mitochondria harms proteins, lipids, and nucleic acids, among other cellular constituents. Most ROS generated during aerobic metabolism can be eliminated by a number of antioxidant enzymes and small molecular weight antioxidants found in cells and mitochondria, under normal physiological conditions[4,5].

Long-term (LT) consumption of D-galactose (D-gal), present in a variety of foods including milk and dairy products, chocolate, and honey, has been demonstrated to induce alterations that mimic the aging process that occurs naturally in animals[6]. D-galactokinase or galactose-1-phosphate uridyltransferase usually metabolizes D-gal in mammals; However, aberrant metabolism is brought on by excessive D-gal. During this process, D-gal is changed into galactitol, which can build up inside the cell and cause osmotic stress and ROS. The reduced form of nicotine adenine dinucleotide phosphate causes a decrease in glutathione (GSH) reductase activity, while excess D-gal also leads to the production of galactitol by aldose reductase activity. Consequently, the cell experiences a build-up of free radical species, including hydrogen peroxide, leading to severe oxidative damage. Furthermore, galactose oxidase can catalyze the conversion of large concentrations of D-gal to aldose hydroperoxides, which form ROS and superoxide anions. Cellular damage and oxidative stress are caused by all of these metabolic mechanisms[7,8].

Boron, a bioactive non-metal, is in group 3A in the periodic table. Boric acid (BA) is found in nature as the sassolite mineral. It is stated that when dietary boron compounds are taken orally, they are rapidly biotransformed into BA in the gastrointestinal tract, and almost all of them are absorbed as BA and transported to the tissues via the blood[9]. BA is a dynamic trace element needed by many organisms, including humans, for biological and metabolic activities and plays significant roles. But its exact biochemical mode of action is still unknown. It is generally hypothesized that it could affect vital biochemical processes such as oxidative stress, energy metabolism, endocrine activities, and the metabolism of bones and minerals. Dietary BA sources are plant-based and are mostly found in fruits such as dried apricots, raisins, almonds, hazelnuts, avocados, chickpeas, quince, wine, vine leaves, parsley, and peaches[10,11]. BA interacts with hydroxyl groups in serine structures, with N in histidine's imidazole group, or with cis-hydroxyl groups on the ribosyl segments of nucleotides and with serine proteases in both humans and higher animals. These interactions may affect the regulation of specific metabolic pathways and enzymatic activity of serine proteases or oxidoreductases that require pyridine or flavin nucleotides[10].

Studies have shown that BA has antioxidant effects, strengthens the immune system, regulates energy metabolism and calcium, plays a role in bone growth and wound healing, increases mental performance, the amount of reduced GSH in the body, and reduces oxidative damage[12,13]. Since it has been used safely in previous experimental studies, we used 100 mg/kg for the BA dose in our study. The acute LD_{50} value of BA was found to be 3450 mg/kg for mice and 2660 mg/kg for rats using biochemical analyses[14,15].

In this study, we assessed BA's protective effects on oxidative stress and cognitive functioning using a mimetic aging model.

MATERIALS and METHODS

Chemicals

D-gal and BA were purchased from Sigma-Aldrich (St. Louis, MO, USA).

Animal Studies

Thirty-two male Wistar albino rats, aged three months, were used in the investigation. The rats were housed in typical cages with a 12-hour light and dark cycle at a temperature of 22±2 °C. Standard pellet feed was given to the rats on an ad libitum basis. This investigation was conducted in the laboratory of the Üsküdar University Experimental Research Unit. The Üsküdar University Animal Experiments Ethics Committee approved the study protocol (approval no: 2021-10, date: 24.12.2021).

Experimental Procedure

The animals were divided into four groups. The eight rats in the control group were fed commercial rat chow. At the same time, the animals in the D-gal group (n=8) received 150 mg/kg/day of D-gal subcutaneously (s.c.); The animals in the BA group (n=8) received 100 mg/kg/day of BA by oral gavage; and the animals in the D-gal+BA group (n=8) received a combination of D-gal (150 mg/kg/day) by s.c. injection and BA (100 mg/kg/day) by oral gavage during 12 weeks. In our study, the BA dose was estimated by Kar et al.[14] using a specific reference, while the D-gal dose was determined by Çoban et al.[16].

Novel Object Recognition Test

The novel object recognition test (NORT) uses identical objects with varying colors and shapes in four stages to assess the short-term (ST) and long-term visual memory of rats: habituation, retention, ST memory, and LT memory sessions. The animals were accustomed to an empty apparatus during the habituation stage, after which two identical objects were placed there. Two hours later, the ST memory phase began, replacing one object with another. After 24 hours, the LT memory phase began, replacing the object changed in the previous phase with another object. To avoid odor interference between tests, ethyl alcohol was used to clean the objects and test apparatus. The capacity of rats to distinguish between familiar and new objects was measured using the discrimination index (DI) and recognition index (RI). These indexes suggest that healthy animals should spend more time examining unfamiliar objects. The reference was used to calculate DI and RI[17].

Morris Water Maze

Morris Water Maze (MWM) is one of the preferred tests when evaluating learning and memory performance (especially hippocampus-dependent). The iterative process of teaching the platform's location is known as the learning phase. During the testing phase, the elevated platform's previously taught position should be identified, and the platform should be guided to its previously taught position. There are guiding clues placed throughout the tank to aid in the learning process. Water fills the tank, which has a 150 cm diameter and a 60 cm height. Measurements are taken via video and the image is transferred to the monitor via the camera system mounted on the tank (SMART 3.0)[18].

The platform is positioned in a randomly chosen quadrant (northwest, northeast, southwest, or southeast) created by dividing the final image. The rats were let go into the water from their assigned quadrants for five days, and they had up to 120 seconds to locate the platform. Rats that could not find the platform were directed to the platform and removed, and then kept on the platform for 15 seconds. On the 6th day, the rats were left in the water, the platform was removed, and measurements were made using the system.

Preparation of Serum and Brain Tissue Samples

After the 12-week trial was over, blood was drawn from the rats' hearts, and they were then given intramuscular injections of the anesthetic Xylazine (8-10 mg/kg) and ketamine (80-100 mg/kg). After being centrifuged for ten minutes at 3,000 rpm, blood samples were kept at -80 °C. After the brain tissues were swiftly removed, they were gently washed in saline solution (0.9%) and homogenized in cold 0.15 M KCl (10%; W/v). The homogenates were then centrifuged for 15 minutes at 4 °C at 10,000 × g.

Determination of Glutathione Level

The amount of GSH in blood and a homogenized brain tissue sample was determined according to Serdaroğlu Kaşıkçı and Gökalp[19] using metaphosphoric acid for protein precipitation and 5.5'-dithiobis-2-nitrobenzoic acid for color development.

Determination of Malondialdehyde Level

Malondialdehyde (MDA) was assessed as a measure of lipid peroxidation (LPO) in serum and homogenized brain tissue samples. LPO was determined, according to Coban et al.[16], by measuring the MDA content with thiobarbituric acid.

Statistical Analysis

For statistical analysis, GraphPad Prism version 10.0.0 for Windows (GraphPad Software, Boston, Massachusetts USA, www.graphpad.com) was utilized. The one-way ANOVA test was used to compare the groups, and the LSD test was used for post-hoc pair comparison. The p-values denote different levels of significance: less than 0.05 indicates significant, less than 0.01 indicates highly significant, and less than 0.001 indicates very highly significant, respectively.

RESULTS

The effects of BA on the levels of GSH and MDA in serum are displayed in Figure 1.

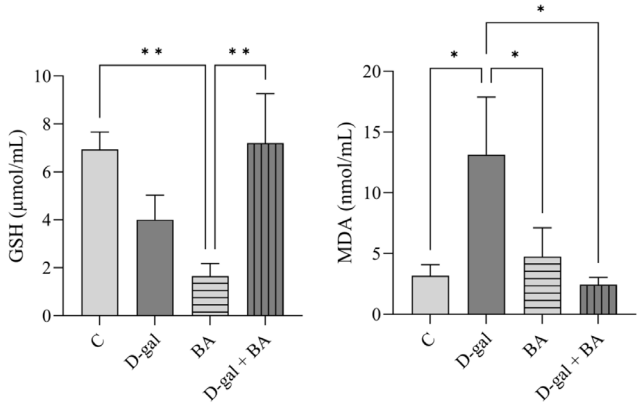

Figure 1. Effects of BA administration on serum GSH and MDA levels in D-gal treated rats.

*p<0.05, **p<0.01, C: Control, D-gal: D-galactose, BA: Boric acid, MDA: Malondialdehyde, GSH: Glutathione

Although not statistically significant, the D-gal group's serum GSH levels dropped in comparison to the control group. However, it was demonstrated that BA raised serum GSH in comparison to D-gal+BA (p=0.0046) and lowered its levels in comparison to the control group (p=0.0066). In addition, when compared to the control group (p=0.0169), the D-gal group was shown to have higher serum MDA levels; In contrast, the BA (p=0.0401) and D-gal+BA (p=0.0111) groups had lower MDA levels (Figure 1).

Figure 2 shows the impact of BA on brain homogenates' levels of GSH and MDA. GSH levels were found to be lower in the D-gal group compared with the control group (p=0.0276). Conversely, it was shown that the D-gal+BA group had higher GSH levels. There were increases in GSH levels in both the D-gal+BA and BA groups as compared to the Control group (p=0.0049, p=0.0014) (Figure 2).

Furthermore, MDA levels were found to be higher in the D-gal group than in the control group (p<0.0001). However, the BA (p=0.0039) and D-gal+BA (p<0.0001) group's MDA levels were found to be lower than those of D-gal. The D-gal group that received BA had lower MDA levels compared to the group that received only BA (p=0.0083) (Figure 2).

In comparison to the control group, subjects treated with D-gal were found to have a lower ST RI (p=0.0414) (Figure 3).

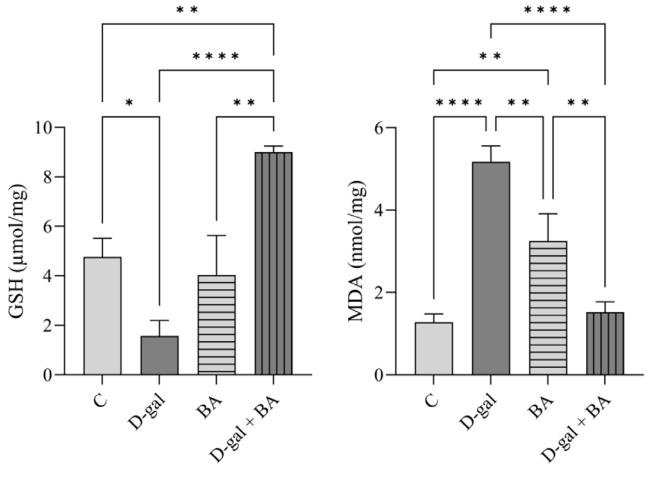

Figure 2. Effects of BA administration on brain homogenates GSH and MDA levels in D-gal treated rats.

*p<0.05, **p<0.01, ****p<0.0001, C: Control, D-gal: D-galactose, BA: Boric acid

It was shown that there was a decrease in the ST DI of D-gal compared to the control group (p=0.0466), whereas it was increased in the BA group (p=0.0237) (Figure 4).

When D-gal and the Control group's times to reach the platform in the Morris water tank were compared, it was found that the D-gal's time increased (p<0.0001), but the BA and the D-gal+BA groups' times decreased (p<0.0001) (Figure 5).

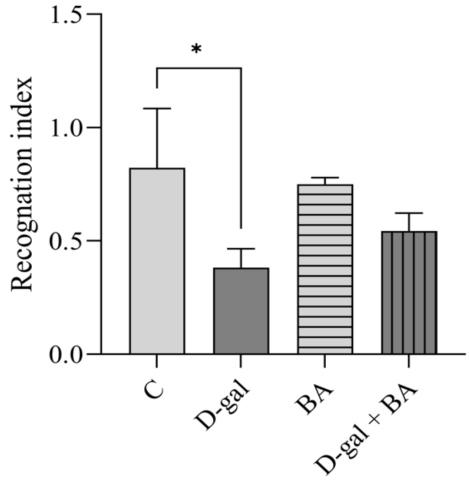

Figure 3. Short-term recognition index in the new object recognition test.

*p<0.05, C: Control, D-gal: D-galactose, BA: Boric acid

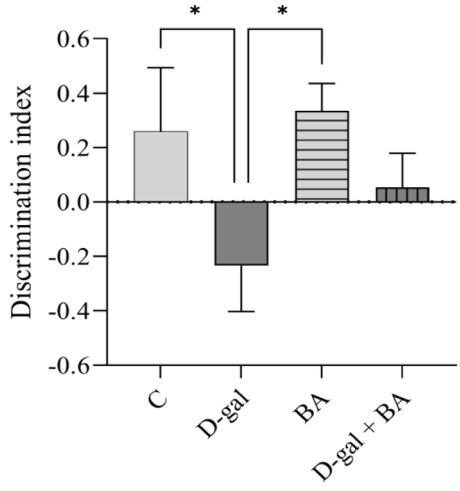

Figure 4. Short-term discrimination index in the novel object recognition test.

*p<0.05, C: Control, D-gal: D-galactose, BA: Boric acid

In the MWM, the D-gal+BA group spent more time in the target quadrant than the D-gal (p=0.017) and BA (p=0.0183) groups (Figure 6).

There was a reduction in the time required to locate the platform in the MWM test the BA and D-gal+BA groups showed shorter platform-finding times than the D-gal group (p=0.0253), while the control group (p=0.0475) experienced longer platform-finding times (Figure 7).

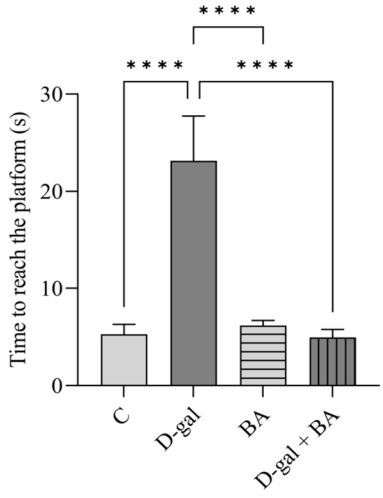

Figure 5. Time to reach the platform in Morris water maze.

****p<0.0001, C: Control, D-gal: D-galactose, BA: Boric acid

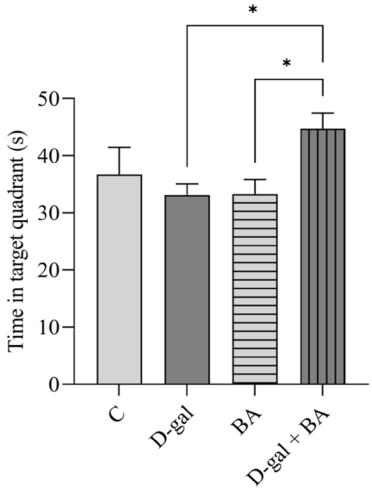

Figure 6. Time spent in the platform quadrant in Morris water maze.

*p<0.05, C: Control, D-gal: D-galactose, BA: Boric acid

DISCUSSION

Neurodegenerative diseases may be caused by the brain aging rapidly. Because of its high lipid content, high metabolic activity, and weak antioxidant defense mechanisms, the brain is an organ that is particularly vulnerable to oxidative damage. Free radical generation and antioxidants are in balance in healthy people and other organisms under typical physiological conditions. However, as we age, this balance is disturbed, which increases the generation of free radicals and gradually reduces the effectiveness of the antioxidant defense system[20]. In some studies, LT D-gal administration led to cognitive and motor deficits, which provided an animal model of aging similar to that of humans[21].

Studies conducted by administering D-gal have shown that brain LPO levels increase, and this leads to DNA damage and a decrease in antioxidant systems. Studies have shown that an aging model can be induced by administering D-gal (100-500 mg/kg/day)[16,22]. Hence, we have chosen rats as the experimental animals, determine the dosage, and set up the experimental groups. D-gal treatment in rodents was shown in some investigations to raise MDA levels in brain tissue samples and reduce GSH levels in serum. Furthermore, histological alterations were also observed, along with disturbances in memory and learning[7,12]. According to a recent study, various boron compounds raised antioxidant enzyme activity at modest supplement levels without putting blood cells under oxidative stress. Conversely, exposure to D-gal was found to significantly reduce the antioxidant enzyme activities of the rat brain's neurons and glial cells. Additionally, the direct impact of D-gal on enzyme

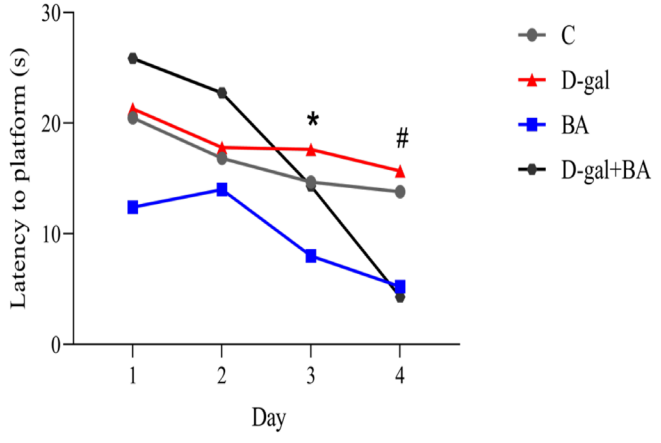

Figure 7. Four-day platform reach time in Morris water maze.

*p<0.05, #p<0.05, C: Control, D-gal: D-galactose, BA: Boric acid

molecules or their formation was accompanied by an increase in oxidative stress. Therefore, a decline in antioxidant activity may lead to the development of certain neurodegenerative diseases. In many studies conducted on various boron compounds[12]. Boron can behave as an indirect proton donor and has a special effect on the structure and function of cell membranes. Accordingly, it has been claimed that cyclic adenosine monophosphate, whose concentration increases when boron is present, can disrupt mitochondrial oxidative phosphorylation metabolism and suppress the activity of hydrolytic enzymes[9,10,13]. Herein, the antioxidant properties of boron compounds, like BA, that have been studied in neural cells may be related to their important functions in mitochondrial dynamics.

Kar et al.[14] assessed the effects of various BA dosages on kidney tissue using an ischemia-reperfusion model. Following three distinct intraperitoneal doses of 50, 100, and 200 mg/kg BA, they found that the administration of 200 mg/kg BA reduced MDA levels in the kidney tissue while elevating GSH, superoxide dismutase, and Catalase levels[14]. It was reported that administering 50 mg/kg of BA for 35 days decreased oxidative stress in a study utilizing a Parkinson's model[13]. Conivaptan and BA combined treatment was found to raise GSH levels and lower MDA levels in comparison to the control group in a study on acute renal damage[23]. In comparison to the control group, the D-gal treated group had higher MDA and lower GSH levels in both serum and brain homogenates. However, we found that the dosage applied in the BA group did not significantly increase GSH levels compared to antioxidants such as quercetin and vitamin C in both serum and brain homogenates compared to the control. Moreover, BA might modulate the cell's own antioxidant defense mechanisms, causing a pro-oxidant effect. When we compared the data between D-gal and D-gal+BA, we observed that while the GSH level raised in both groups, MDA levels dropped in the D-gal+BA group. All the results obtained were statistically significant, as seen in Figures 1 and 2.

In the current investigation, we used a NORT and a MWM to evaluate non-aversive learning and spatial memory in rats administered BA and D-gal. Özdemir et al.[15] evaluated the effects of BA on brain tissue in an experimental Alzheimer's model. The results of the radial arm maze test indicated that BA (200 mg/kg) reduced the damage to learning and memory functions in this model. In addition, it was reported that BA dramatically lowered oxidative stress markers and that total antioxidant capacity levels rose in the BA group and declined in the Alzheimer group[15]. Furthermore, Cui et al.[24] reported that D-gal can cause behavioral impairment in C57BL/6J mice, and Reitz et al.[25] reported that D-gal can reduce spatial preference for the target quadrant in the MWM test.

Similar to the studies of Khan et al.[18] and Kaviani et al.[26] in our study, we found that the ST recognition and DI in the NORT was significantly reduced in the D-gal applied group compared to the control. However, BA reversed the working memory and desire for novelty deficits caused by D-gal. As a result, both RI and DI were found to be higher in the D-gal+BA group compared to the D-gal group (Figures 3 and 4).

Changes in redox state play a critical role in aging and the resulting decrease in memory[27,28]. D-gal treatment resulted in memory impairment, and the MWM test showed longer escape latency. According to the MWM test results in the aging model created by Samad et al.[29] by administering D-gal, the number of rats reaching the platform increased in the D-gal group compared to the control. We also obtained similar results in our study (Figure 5). Zhang et al.[21] showed, that the time spent in the target quadrant in the MWM test decreased in the Alzheimer's model induced by D-gal and aluminum chloride. Similarly, in our study, we found that the time spent in the target quadrant decreased in the D-gal group compared to the control group, although this time was not statistically significant. There was, however, a statistically significant increase in the D-gal+BA groups compared to the BA and D-gal groups (Figure 6). Consistent with the study of Zhang et al.[21], an increase in the latency period was observed in our study in the D-gal group compared to the control group[21]. MWM testing illustrated the increased latency of rats, consistent with previous research by Wang et al.[30], indicating successful aging modeling. In contrast, we detected an increase in the latency period in the D-gal+BA group compared to the D-gal group. According to this finding, BA may help the cognitive deficits seen in the mimetic aging model[30].

Study Limitation

In light of this, individuals with underlying medical conditions that mimic normal aging, as well as the elderly, should consume fewer foods high in D-gal. The current investigation additionally revealed that D-gal-induced brain aging and cognitive impairment in young rats were prevented by administering BA. According to these findings, a diet high in D-gal may cause or hasten the aging process, but regular lifestyle changes can stop this from happening. Hence, further clinical studies are needed to understand how D-gal and BA affect brain aging, neurotoxicity, and cognitive functions. In the current study, different doses of BA should be tried

and examined in detail with molecular and histological studies. This is the limitation of our study.

CONCLUSION

Our study revealed that BA reduces oxidative damage by lowering LPO levels in the mimetic aging model. BA improved the ST DI in the NORT and had positive effects on memory by reducing the time to reach the platform and the time spent on the platform in the MWM. However, further studies are needed on the effects of BA on aging-related neurodegenerative disorders, involving different doses. At the same time, we foresee benefiting from its anti-aging properties by consuming foods containing BA.

Ethics

Ethics Committee Approval: This study was approved by the Üsküdar University Animal Experiments Ethics Committee (approval no: 2021-10, date: 24.12.2021).

Informed Consent: Since this study is on animals, patient consent is not required.

Foonotes

Authorship Contributions

Surgical and Medical Practices: E.S.K., B.Ç., F.N.S., Concept: E.S.K., B.Ç., F.N.S., Z.G., A.S., Design: E.S.K., B.Ç., Data Collection or Processing: E.S.K., B.Ç., Z.G., A.S., R.S., Analysis or Interpretation: E.S.K., B.Ç., F.N.S., Z.G., A.S., R.S., Literature Search: E.S.K., B.Ç., A.S., R.S., Writing: E.S.K., B.Ç.

Conflict of Interest: No conflict of interest was declared by the authors.

Financial Disclosure: The authors declare that this study received no financial support.

REFERENCES

1. Balazy M, Nigam S. Aging, lipid modifications and phospholipases--new concepts. Ageing Res Rev. 2003;2:191-209.
2. Gilca M, Stoian I, Atanasiu V, Virgolici B. The oxidative hypothesis of senescence. J Postgrad Med. 2007;53:207-13.
3. Kumar A, Prakash A, Dogra S. Neuroprotective effect of carvedilol against aluminium induced toxicity: possible behavioral and biochemical alterations in rats. Pharmacol Rep. 2011;63:915-23.
4. Ali HA, Afifi M, Abdelazim AM, Mosleh YY. Quercetin and omega 3 ameliorate oxidative stress induced by aluminium chloride in the brain. J Mol Neurosci. 2014;53:654-60.
5. Bitmez B, Çevreli B, Kaşikçi E. Effect of thymol on oxidative stress and reelin signaling pathway in Alzheimer's disease model. Turk J Biol. 2024;48:70-9.
6. Azman KF, Zakaria R. D-Galactose-induced accelerated aging model: an overview. Biogerontology. 2019;20:763-82.
7. Serdaroglu Kasikci E. Evaluation of longterm quercetin administration on age related oxidative stress induced by d-galactose in rats. Fres Environ Bull. 2018;27:7781-6.
8. Pantiya P, Thonusin C, Ongnok B, et al. Chronic D-galactose administration induces natural aging characteristics, in rat's brain and heart. Toxicology. 2023;492:153553.
9. Khaliq H, Juming Z, Ke-Mei P. The physiological role of boron on health. Biol Trace Elem Res. 2018;186:31-51.
10. Ayhanci A, Tanriverdi DT, Sahinturk V, Cengiz M, Appak-Baskoy S, Sahin IK. Protective effects of boron on cyclophosphamide-induced bladder damage and oxidative stress in rats. Biol Trace Elem Res. 2020;197:184-91.
11. Barrón-González M, Montes-Aparicio AV, Cuevas-Galindo ME, et al. Boron-containing compounds on neurons: actions and potential applications for treating neurodegenerative diseases. J Inorg Biochem. 2023;238:112027.
12. Coban FK, Ince S, Kucukkurt I, Demirel HH, Hazman O. Boron attenuates malathion-induced oxidative stress and acetylcholinesterase inhibition in rats. Drug Chem Toxicol. 2015;38:391-9.
13. Yavuz E, Çevik G, Çevreli B, Serdaroğlu Kaşıkçı E. Effect of boric acid and quercetin combination on oxidative stress/ cognitive function in parkinson model. J Boron. 2023;8:85-91.
14. Kar F, Hacioglu C, Senturk H, Donmez DB, Kanbak G. The role of oxidative stress, renal inflammation, and apoptosis in post ischemic reperfusion injury of kidney tissue: the protective effect of dose-dependent boric acid administration. Biol Trace Elem Res. 2020;195:150-8.
15. Özdemir Ç, Arslan M, Küçük A, Yığman Z, Dursun AD. Therapeutic efficacy of boric acid treatment on brain tissue and cognitive functions in rats with experimental alzheimer's disease. Drug Des Devel Ther. 2023;17:1453-62.
16. Çoban J, Doğan-Ekici I, Aydın AF, Betül-Kalaz E, Doğru-Abbasoğlu S, Uysal M. Blueberry treatment decreased D-galactose-induced oxidative stress and brain damage in rats. Metab Brain Dis. 2015;30:793-802.
17. Lueptow LM. Novel object recognition test for the investigation of learning and memory in mice. J Vis Exp. 2017;126:55718.
18. Khan MZ, Atlas N, Nawaz W. Neuroprotective effects of Caralluma tuberculata on ameliorating cognitive impairment in a d-galactose-induced mouse model. Biomed Pharmacother. 2016;84:387-94.
19. Serdaroğlu Kaşıkçı E, Gökalp HK. The effect of kefir on oxidative stress in the brain tissue of aging modeled rats by D-galactose inducement. J Natural and Applied Sci. 2018;22:221-8.
20. Tsai SJ, Yin MC. Anti-oxidative, anti-glycative and anti-apoptotic effects of oleanolic acid in brain of mice treated by D-galactose. Eur J Pharmacol. 2012;689:81-8.
21. Zhang Z, Wu H, Qi S, et al. 5-Methyltetrahydrofolate alleviates memory impairment in a rat model of Alzheimer's disease induced by D-galactose and aluminum chloride. Int J Environ Res Public Health. 2022;19:16426.
22. Garg G, Singh S, Singh AK, Rizvi SI. Antiaging effect of metformin on brain in naturally aged and accelerated senescence model of rat. Rejuvenation Res. 2017;20:173-82.
23. Can B, Kar F, Kar E, et al. Conivaptan and boric acid treatments in acute kidney injury: is this combination effective and safe? Biol Trace Elem Res. 2022;200:3723-37.
24. Cui X, Zuo P, Zhang Q, et al. Chronic systemic D-galactose exposure induces memory loss, neurodegeneration, and oxidative damage in mice: protective effects of R-alpha-lipoic acid. J Neurosci Res. 2006;83:1584-90.

25. Reitz C, Luchsinger J, Tang MX, Manly J, Mayeux R. Impact of plasma lipids and time on memory performance in healthy elderly without dementia. Neurology. 2005;64:1378-83.

26. Kaviani E, Rahmani M, Kaeidi A, et al. Protective effect of atorvastatin on D-galactose-induced aging model in mice. Behav Brain Res. 2017;334:55-60.

27. Upright NA, Baxter MG. Prefrontal cortex and cognitive aging in macaque monkeys. Am J Primatol. 2021;83:e23250.

28. Aguilar-Hernández L, Vázquez-Hernández AJ, de-Lima-Mar DF, Vázquez-Roque RA, Tendilla-Beltrán H, Flores G. Memory and dendritic spines loss, and dynamic dendritic spines changes are age-dependent in the rat. J Chem Neuroanat. 2020;110:101858.

29. Samad N, Azdee MAH, Imran I, Ahmad T, Alqahtani F. Mitigation of behavioral deficits and cognitive impairment by antioxidant and neuromodulatory potential of Mukia madrespatana in D-galactose treated rats. Saudi J Biol Sci. 2023;30:103708.

30. Wang YJ, Wang XY, Hao XY, et al. Ethanol extract of centipeda minima exerts antioxidant and neuroprotective effects via activation of the Nrf2 signaling pathway. Oxid Med Cell Longev. 2019;2019:9421037.

DOI: 10.4274/MMJ.galenos.2025.37209
Medeni Med J 2025;40:26-30

Case Report

Ocular Manifestations of Kaposi Sarcoma: Insights from an HIV-Positive Patient and an Immunocompetent HIV-Negative Patient

Kaposi Sarkomunun Göz Bulguları: HIV Pozitif Bir Hasta ve İmmun kompetan HIV Negatif Bir Hastada Sonuçlar

Ebubekir DURMUS[1], Esma Ecem ERSOY[1], Ulviyya ASKEROVA[1], Fatma YILMAZER[2]

[1]Istanbul Medeniyet University Faculty of Medicine, Department of Ophthalmology, Istanbul, Türkiye
[2]Istanbul Medeniyet University Faculty of Medicine, Department of Pathology, Istanbul, Türkiye

ABSTRACT

Kaposi sarcoma (KS) is a vascular neoplasm caused by human herpes virus-8 and is commonly associated with immunocompromised states such as acquired immunodeficiency syndrome. While ocular involvement is rare and typically occurs in human immunodeficiency virus (HIV)-positive patients, it can exceptionally present in HIV-negative, immunocompetent individuals. This report presents two cases of conjunctival KS: One in an HIV-positive patient and another in an HIV-negative patient. The patients were diagnosed and followed up at Istanbul Medeniyet University Göztepe Prof. Dr. Süleyman Yalçın City Hospital. Written informed consent was obtained from the patients for the preparation of this case report. A 35-year-old HIV-positive male with a history of cutaneous and genital KS presented with a painless, reddish, hemorrhagic mass on the left inferior fornix and a firm mass on the lower eyelid. Surgical excision with adjuvant cryotherapy and amniotic membrane transplantation was performed. One year postoperatively, no recurrence or new lesions were observed. A 76-year-old immunocompetent female presented with a painless, progressively enlarging mass in the left inferior fornix. She underwent surgical excision, adjuvant cryotherapy, and amniotic membrane transplantation. Histopathology confirmed the diagnosis of KS, and at the 1-year follow-up, no recurrence or new lesions were observed. Ocular KS, though rare, can occur in both immunocompromised and immunocompetent individuals. This report highlights the importance of considering KS in the differential diagnosis of subconjunctival hemorrhage, even in patients without underlying immunosuppressive conditions. Both cases were successfully managed with surgical excision, adjuvant cryotherapy, and amniotic membrane transplantation, with no recurrence during follow-up.

Keywords: Ocular kaposi sarcoma, subconjunctival hemorrhage, HIV positive patient, HIV negative patient

ÖZ

Kaposi sarkomu (KS), insan herpes virüsü-8 tarafından oluşturulan vasküler bir neoplazm olup, genellikle edinilmiş bağışıklık yetersizliği sendromu gibi immun yetmezlik durumlarıyla ilişkilidir. Oküler tutulumu nadir olmakla birlikte, genellikle insan bağışıklık yetmezliği virüsü (HIV)-pozitif hastalarda görülürken, nadiren HIV-negatif, immun kompetan bireylerde de ortaya çıkabilir. Bu olgu sunumu, bir HIV-pozitif hasta ve bir HIV-negatif hasta olmak üzere iki konjunktival KS olgusunu sunmaktadır. Hastalar Istanbul Medeniyet Üniversitesi Göztepe Prof. Dr. Süleyman Yalçın Şehir Hastanesi'nde tanı almış ve takip edilmiştir. Bu olgu raporunun hazırlanması için hastalardan yazılı bilgilendirilmiş onam alınmıştır. Olgu sunumları: Olgu 1: Otuz beş yaşındaki HIV-pozitif erkek hasta, deri ve genital KS öyküsü ile birlikte sol inferior fornikste ağrısız, kırmızı, kanamalı bir kitle ve alt göz kapağında sert bir kitle ile başvurdu. Cerrahi eksizyon, adjuvan kriyoterapi ve amniyotik membran transplantasyonu yapıldı. Operasyondan bir yıl sonra, nüks veya yeni lezyonlar gözlemlenmedi. Olgu 2: Yetmiş altı yaşındaki immun kompetan kadın hasta, sol inferior fornikste ağrısız, giderek büyüyen bir kitle ile başvurdu. Cerrahi eksizyon, adjuvan kriyoterapi ve amniyotik membran transplantasyonu gerçekleştirildi. Histopatolojik inceleme KS tanısını doğruladı ve bir yıl sonraki takipte nüks veya yeni lezyonlar gözlemlenmedi. Oküler KS, nadir olmasına rağmen, hem immun yetmezlik durumunda hem de immun kompetan bireylerde görülebilir. Bu rapor, subkonjunktival kanama durumunda KS'yi ayırıcı tanıda göz önünde bulundurmanın önemini vurgulamaktadır; bu, immun baskılayıcı durumları olmayan hastalarda bile geçerlidir. Her iki olgu da cerrahi eksizyon, adjuvan kriyoterapi ve amniyotik membran transplantasyonu ile başarılı bir şekilde yönetilmiş ve takip sırasında nüks gözlemlenmemiştir.

Anahtar kelimeler: Oküler kaposi sarkomu, subkonjonktival kanama, HIV pozitif hasta, HIV negatif hasta

Address for Correspondence: E. E. Ersoy, Istanbul Medeniyet University Faculty of Medicine, Department of Ophthalmology, Istanbul, Türkiye
E-mail: esmaecemersoy@gmail.com **ORCID ID:** orcid.org/0000-0002-9563-1846

Cite as: Durmus E, Ersoy EE, Askerova U, Yilmazer F. Ocular manifestations of kaposi sarcoma: insights from an HIV-positive patient and an immunocompetent HIV-negative patient. Medeni Med J. 2025;40:26-30

Received: 19 October 2024
Accepted: 14 January 2025
Epub: 29 January 2025
Published: 28 March 2025

INTRODUCTION

Kaposi sarcoma (KS) is a vascular neoplasm caused by human herpes virus 8 (HHV-8), regarded as an acquired immunodeficiency syndrome (AIDS)-defining illness due to its opportunistic nature and frequent occurrence in immunocompromised individuals. It commonly presents in patients with a CD4+ lymphocyte count below 500 cells/µl, particularly under 200 cells/µL[1]. Clinically, KS manifests as a spectrum ranging from indolent, low-grade lesions to purplish-red tumors, which may affect various body regions and develop into fatal, multisystemic angioproliferative malignancies[2]. The global incidence of KS has risen, paralleling the increasing prevalence of AIDS[3]. In addition, KS has been observed in patients undergoing immunosuppressive therapy following organ transplantation[4]. Ocular involvement in KS is rare and primarily associated with AIDS[5]. Between 4% and 12% of AIDS-related KS cases involve ocular manifestations, most commonly affecting the conjunctiva and eyelids[6]. However, ocular KS in human immunodeficiency virus (HIV)-seronegative individuals is exceedingly rare[7].

In this report, we present two cases of conjunctival KS: One in an HIV-seropositive patient with concurrent skin, eyelid, and conjunctival involvement, and another in an HIV-seronegative patient with recurrent conjunctival KS. The HIV-seronegative case is particularly notable, as it represents KS in an immunocompetent individual without any underlying immunosuppressive condition. Both patients underwent surgical excision, cryotherapy, and amniotic membrane transplantation. At the 1-year postoperative follow-up, no recurrence was observed in either patient.

CASE REPORTS

Case 1

A 35-year-old HIV-positive bisexual male presented with a three-month history of a mass on his left lower eyelid. Prior to this, he had lesions on his nose and genital area, diagnosed as KS via biopsy. At presentation, his CD4 cell count was 93 cells/mL, CD8 cell count was 1825 cells/mL, CD4/CD8 ratio was 0,050 and HIV polymerase chain reaction was 61 copies/mL; he was also receiving anti-retroviral therapy with a combination of bictegravir, emtricitabine, and tenofovir. Visual acuity was 6/6 in both eyes. Examination revealed a firm, immobile mass measuring approximately 4x4 mm on the left lower eyelid, extending to the ciliary margin, and a hemorrhagic vascular lesion measuring 8x3 mm on the palpebral conjunctiva with the patient reporting no pain. Surgical excision of conjunctival lesions, along with cryotherapy and amniotic membrane transplantation, and cryotheraphy for the lower eyelid was recommended. The surgery was performed under local anesthesia. The vascularized conjunctival mass was excised with a 3 mm margin, and cryotherapy was applied to the conjunctival margins and eyelid mass. The conjunctival defect was covered with an amniotic membrane graft secured with 10/0 nylon sutures. Histopathological examination confirmed conjunctival KS with positive staining for HHV-8, CD31, and CD34, and approximately 5-15% of cells were positive for Ki67 (Figure 1). At the 1-year postoperative follow-up, the palpebral conjunctiva appeared normal, with regression of the lower eyelid mass. There was no recurrence or new ocular lesions, and systemic involvement was ruled out with biannual positron emission tomography-computed tomography (PET-CT) scans. Figure 2 illustrates the clinical appearance of KS in the palpebral conjunctiva and eyelid, along with the postoperative outcome.

Case 2

A 76-year-old female with a history of glaucoma presented with a progressively enlarging mass in her left lower eyelid, which had been present for approximately one month. Slit-lamp examination revealed a hemorrhagic, raised lesion measuring about 10x3 mm in

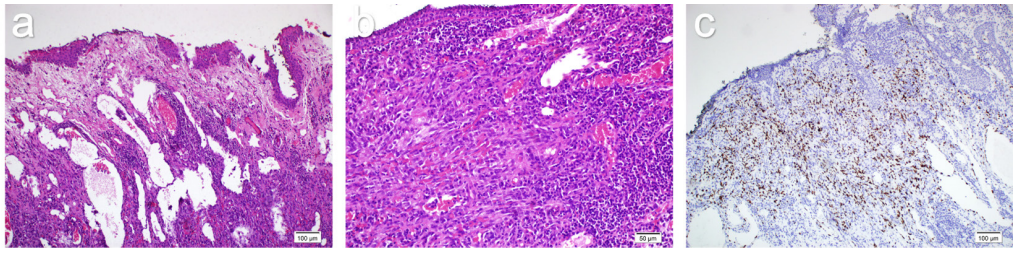

Figure 1. This is the pathology slide of the patient with positive HIV serology. Hematoxylin and eosin staining at x10 magnification (a). Hematoxylin and eosin staining at x20 magnification revealed widespread extravasated erythrocytes outside the vessels. Lymphocytic infiltrates containing plasma cells are present within and around the lesion in most cases (b). Positive nuclear expression was observed in HHV-8 immunohistochemical analysis (c).

HIV: Human immunodeficiency virus, HHV-8: Human herpes virus 8

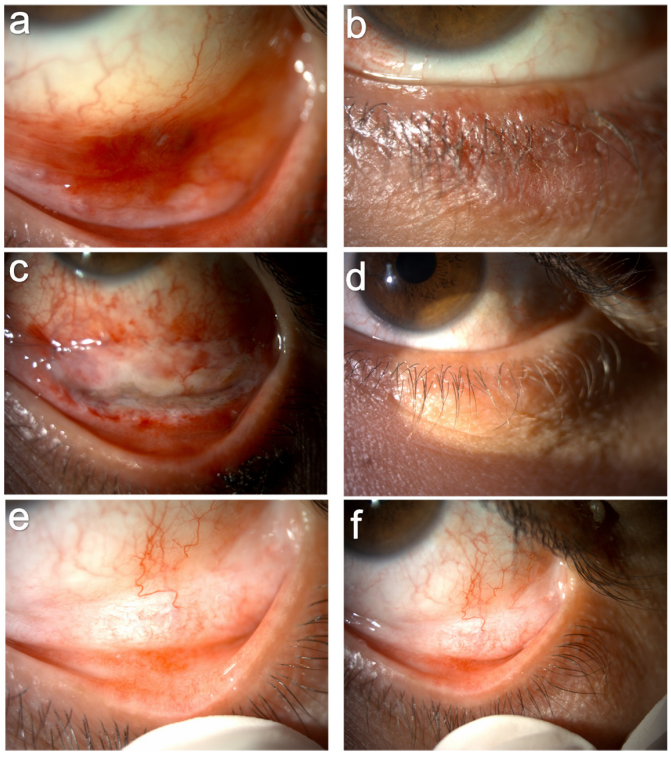

Figure 2. The clinical appearance of KS in the palpebral conjunctiva and eyelid is characterized by a painless, reddish lesion resembling a subconjunctival hemorrhage, flat with a nodular component in the lower fornix (a), and a vascularized, immobile, and rigid mass at the eyelid margin in same patient (b). The conjunctival lesion was surgically excised, followed by cryotherapy and amniotic membrane transplantation (c). The eyelid lesion was treated with cryotherapy alone. Following cryotherapy, the eyelid lesion showed regression of vascularization and shrinkage (d). No recurrence or new lesions were observed at either of the postoperative follow-ups within the first year (e,f).

the left inferior fornix. The patient reported no history of immunosuppressive therapy, high-risk sexual behavior, or intravenous drug use. Hematological and biochemical tests were within normal limits, with no evidence of immunosuppression. Both B- and T-cell counts were normal, and repeated HIV tests were negative. Other serological markers, including anti-hepatitis C virus and HBsAg, were also seronegative. A systemic scan was conducted, during which a chest X-ray revealed early signs of chronic obstructive pulmonary disease. In 2020, the patient underwent a punch biopsy for angiomatous lesions in the umbilical region, diagnosed as hemangioma. In 2019, an excisional biopsy of a similar hemorrhagic lesion in the left conjunctiva confirmed the diagnosis of KS. Contrast-enhanced orbital magnetic resonance imaging (MRI) indicated that the conjunctival lesion was localized without orbital infiltration. A surgical excision

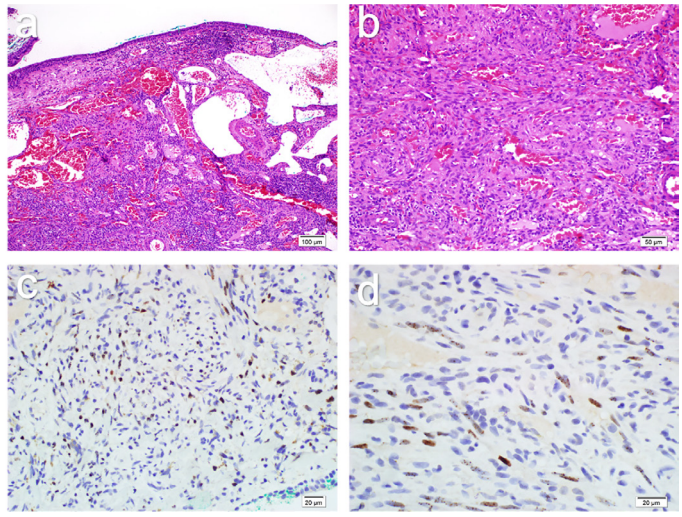

Figure 3. This is the pathology slide image of the patient with negative HIV serology. A nodular lesion composed of spindle cell fascicles observed with hematoxylin and eosin staining at x10 magnification (a). At x20 magnification with hematoxylin and eosin staining, spindle cells are intermingled with sieve-like, slit-shaped, blood-filled vascular structures (b). Patchy immunohistochemical staining of HHV-8 at x40 magnification (c). At x60 magnification, the characteristic paranuclear "dot-like" staining pattern of HHV-8 observed in Kaposi sarcoma (d).

HIV: Human immunodeficiency virus, HHV-8: Human herpes virus 8

of the conjunctival mass, followed by cryotherapy and amniotic membrane transplantation, was performed. Histopathology confirmed KS, showing positive staining for CD31, CD34, and HHV-8, with increased Ki67 activity (Figure 3). The patient was followed for one year, with no recurrence or new conjunctival lesions observed. HIV seroconversion was not detected, and systemic involvement was ruled out through orbital MRI and PET-CT scans. Figure 4 illustrates the clinical appearance of KS and the postoperative outcome.

DISCUSSION

KS manifests in four variants: Classic (Mediterranean), Endemic (African), Iatrogenic (Transplant-related), and AIDS-associated (Epidemic)[8]. This case report highlights the clinical presentation of ocular KS in both HIV-positive and HIV-negative patients. KS, caused by oncogenic HHV-8, is the most common neoplasm in AIDS patients, though ocular involvement is rare[9]. To date, only three cases of ocular KS as an initial manifestation of HIV have been documented, all involving the conjunctiva[10-12]. Ocular KS in HIV-negative individuals is exceedingly uncommon[13]. Ocular KS typically presents as a raised, reddish-brown mucocutaneous lesion, requiring differentiation from

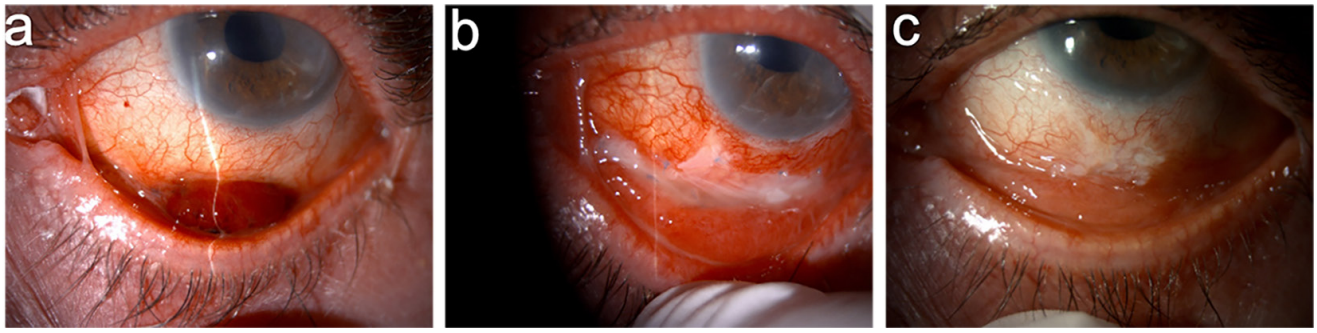

Figure 4. A painless, reddish mass consistent with Kaposi sarcoma was located on the left inferior fornix (a). Surgical excision of the lesion with adjuvant cryotherapy, and amniotic membrane transplantation was performed (b). No recurrence or new lesions were observed during the first-year postoperative follow-up (c).

conditions such as angiosarcoma, hemangioma, and pyogenic granuloma[7]. In the HIV-positive patient, KS developed during ongoing immunosuppression despite anti-retroviral therapy[2].

In contrast, KS in HIV-negative individuals often occurs following immunosuppression due to transplants, but may also arise due to localized immune dysregulation or genetic predispositions, with factors like chronic inflammation, trauma, or ultraviolet radiation triggering HHV-8 activation and promoting angiogenesis[14,15]. Furthermore, genetic variations in immune regulatory genes like vascular endothelial growth factor and IL-6 might also contribute to KS progression[16]. Ocular KS in HIV-negative individuals is rare but should be considered in the differential diagnosis of vascular lesions, particularly in elderly patients; as classic KS, which primarily affects Mediterranean and Eastern European populations, can occur in this group[9]. Despite differences in underlying mechanisms, the clinical manifestations are usually similar. Our HIV-negative patient exhibited no significant immunosuppressive factors, suggesting that advanced age or other underlying factors may play a role in KS development in immunocompetent individuals. The clinical course, disease progression, and treatment outcomes may vary in HIV-negative cases, where localized treatments could be more effective than systemic approaches typically used for HIV-related KS. This highlights the necessity of individualized diagnostic and therapeutic strategies for HIV-negative KS, considering the distinct pathogenic mechanisms.

According to the National Comprehensive Cancer Network guidelines, localized therapies are recommended for minor lesions, and systemic treatments are advised for refractory cases and in advanced disease[17]. Although originally developed for AIDS-related KS, these guidelines are applicable to non-HIV-related cases and emphasize the importance of tailoring treatment strategies to the individual patient's needs. Management typically involves surgical excision, with adjuvant therapy tailored to the severity of the disease and the patient's overall health. Ocular KS affecting the conjunctiva and eyelids generally has a non-aggressive course and can be treated with simple excision[3]. Adjunctive interventions may include radiotherapy, chemotherapy, cryotherapy, amniotic membrane transplantation, and intraoperative mitomycin-C application[2,8,18]. Recently, combined weekly docetaxel and anti-retroviral therapy have been explored as alternatives[19]. In our cases, surgical excision of the conjunctival tumors was followed by cryotherapy and amniotic membrane transplantation, with pathological examination revealing negative surgical margins, thus eliminating the need for further intervention. No systemic involvement was detected through orbital MRI and PET-CT scans, making systemic treatment unnecessary. The HIV-positive patient received only cryotherapy for the eyelid lesion, which demonstrated favorable regression without recurrence or new lesions during follow-up.

CONCLUSION

Ocular KS can occur in both HIV-positive and, rarely, HIV-negative patients. Our second case highlights the need to consider KS in the differential diagnosis of subconjunctival hemorrhage, even in immunocompetent individuals without a history of immunosuppression. Both patients responded well to surgical excision followed by cryotherapy and amniotic membrane transplantation, with no recurrence observed during the 1-year follow-up.

Ethics

Informed Consent: Written informed consent was obtained from the patients for the preparation of this case report.

Footnotes

Author Contributions

Surgical and Medical Practices: E.D., Concept: E.D., Design: E.E.E., U.A., Data Collection and/or Processing: E.E.E., F.Y., Analysis and/or Interpretation: E.E.E., F.Y., Literature Search: E.E.E., U.A., Writing: E.D., E.E.E.

Conflict of Interest: The authors have no conflict of interest to declare.

Financial Disclosure: The authors declared that this study has received no financial support.

REFERENCES

1. Rohner E, Valeri F, Maskew M, et al. Incidence rate of kaposi sarcoma in HIV-infected patients on antiretroviral therapy in southern africa: a prospective multicohort study. J Acquir Immune Defic Syndr. 2014;67:547-54.
2. Yang J, Yin XF, Li YP, et al. Case report of ocular Kaposi's sarcoma. BMC Ophthalmol. 2017;17:143.
3. Yeak J, Iqbal T, Zahari M, et al. Total resolution of ocular Kaposi sarcoma with different treatment approaches - a case series and review of literature. Int J STD AIDS. 2019;30:802-9.
4. Pantanowitz L, Dezube BJ. Kaposi sarcoma in unusual locations. BMC Cancer. 2008;8:190.
5. Tessari G, Naldi L, Boschiero L, et al. Incidence and clinical predictors of Kaposi's sarcoma among 1721 Italian solid organ transplant recipients: a multicenter study. Eur J Dermatol. 2006;16:553-7.
6. Kim JW, Lee DK. Unusual eyelid, periocular, and periorbital cutaneous malignancies. Int Ophthalmol Clin. 2009;49:77-96.
7. Abalo-Lojo JM, Abdulkader-Nallib I, Pérez LM, et al. Eyelid Kaposi sarcoma in an HIV-negative patient. Indian J Ophthalmol. 2018;66:854-5.
8. Temelkova I, Tronnier M, Terziev I, et al. A series of patients with Kaposi sarcoma (mediterranean/classical type): case presentations and short update on pathogenesis and treatment. Open Access Maced J Med Sci. 2018;6:1688-93.
9. Venkateswaran N, Ramos JC, Cohen AK, et al. Spotlight on ocular Kaposi's sarcoma: an update on the presentation, diagnosis, and management options. Expert Rev Ophthalmol. 2021;16:477-89.
10. Schmid K, Wild T, Bolz M, et al. Kaposi's sarcoma of the conjunctiva leads to a diagnosis of acquired immunodeficiency syndrome. Acta Ophthalmol Scand. 2003;81:411-3.
11. Curtis TH, Durairaj VD. Conjunctival Kaposi sarcoma as the initial presentation of human immunodeficiency virus infection. Ophthalmic Plast Reconstr Surg. 2005;21:314-5.
12. Mika K, Pogrzebielski A, Dyduch G, et al. Kaposi sarcoma of the conjunctiva as the first manifestation of HIV infection. Am J Case Rep. 2010;11:64-6.
13. Fossataro F, Iuliano A, Uccello G, et al. A rare case of bilateral conjunctival Kaposi's sarcoma in a HIV-negative patient. Am J Ophthalmol Case Rep. 202131;21-101024.
14. Betkowska-Prokop A, Sulowicz J, Sobaszek-Pitas M, Sulowicz W. [Kaposi's sarkoma in solid organ recipients]. Przegl Lek. 2010;67(7):475-8.
15. Einollahi B. Kaposi sarcoma after kidney transplantation. Iran J Kidney Dis. 2007;1:2-11.
16. Rusu-Zota G, Manole OM, Galeș C, et al. Kaposi sarcoma, a trifecta of pathogenic mechanisms. Diagnostics (Basel). 2022;12:1242.
17. Reid E, Suneja G, Ambinder RF, et al. AIDS-related Kaposi sarcoma, version 2.2019, NCCN Clinical Practice Guidelines in Oncology. J Natl Compr Canc Netw. 2019 Feb;17(2):171-89.
18. Korn BS, Park DJ, Kikkawa DO. Intralesional mitomycin-C for the treatment of conjunctival Kaposi sarcoma. Ophthalmic Plast Reconstr Surg. 2011;27:88-90.
19. Jin C, Minhas H, Kaur A, Kodali S, Gotlieb V. A case of ocular kaposi's sarcoma successfully treated with highly active antiretroviral therapy (HAART) combined with docetaxel. Am J Case Rep. 2018;19:1074-7.

DOI: 10.4274/MMJ.galenos.2025.81486
Medeni Med J 2025;40:31-32

Letter to the Editor

Comment on the "Perivascular Invasion: A Promising Prognostic Parameter for Breast Cancer"

"Perivasküler İnvazyon: Meme Kanserinde Umut Verici Prognostik Parametre" Üzerine Yorum

Ahmet BOZER

Izmır City Training and Research Hospital, Clinic of Radiology, Izmır, Türkiye

Keywords: Invasion, prognostic parameter, breast cancer
Anahtar kelimeler: Invasion, prognostic parameter, breast cancer

Dear Editor,

The study titled "Perivascular Invasion: A Promising Prognostic Parameter for Breast Cancer" provides a significant contribution to the understanding of perivascular invasion (PVI) in breast cancer (1). The authors demonstrated that PVI is significantly associated with key clinicopathological parameters, including tumor size, histologic grade, lymphovascular invasion (LVI), and perineural invasion. These findings underscore the potential importance of PVI as a prognostic factor in breast cancer. We read this study with great interest and commend the authors on their valuable contribution.

One of the strengths of this study is its detailed examination of the prognostic significance of PVI. The incorporation of PVI, in addition to commonly used histologic and molecular markers in breast cancer, may enhance risk stratification efforts. The study utilized a large clinicopathological dataset, and the relationships between PVI and several prognostic factors were statistically substantiated. The results reveal that PVI is particularly linked to adverse prognostic indicators, such as larger tumor size and higher histologic grade.

Despite the study's strengths, we believe that certain aspects could benefit from further elaboration. First, the development of a prognostic index incorporating PVI might be worth exploring. In clinical practice, indices such as the Nottingham Prognostic Index are widely used to guide treatment decisions. Including PVI in a similar index could potentially improve the accuracy of clinical risk assessments.

Regarding molecular subtypes, the study found no significant correlation between PVI and breast cancer subtypes. However, as mentioned in the article, previous studies have reported higher microvascular density in certain subtypes, particularly in triple-negative breast cancer. Further research with larger sample sizes may provide more definitive conclusions on this relationship.

In terms of pathological assessment, the study evaluated PVI using only hematoxylin and eosin staining. Given the potential variability in vessel sizes, reliance solely on this method may affect diagnostic accuracy. Incorporating immunohistochemical techniques could enhance diagnostic reliability and reduce interobserver variability.

Address for Correspondence: A. Bozer, Izmır City Training and Research Hospital, Clinic of Radiology, Izmır, Türkiye
E-mail: drahmetbozer@gmail.com **ORCID ID:** orcid.org/0000-0002-0467-741X

Cite as: Bozer A. Comment on the "perivascular invasion: a promising prognostic parameter for breast cancer". Medeni Med J. 2025;40:31-32

Received: 03 February 2025
Accepted: 08 February 2025
Epub: 14 March 2025
Published: 28 March 2025

The study noted that no deaths occurred among patients with PVI during the follow-up period. However, to better assess the prognostic implications of this finding, survival analyses using Kaplan-Meier curves or Cox regression would be beneficial. While the study collected data on overall survival, other critical prognostic outcomes, such as local recurrence and distant metastasis, were not included. Investigating the relationship between PVI and these parameters could provide further insights into its prognostic relevance in clinical practice.

Finally, direct comparisons between PVI and other established prognostic markers, such as LVI and Ki67, would enhance the clarity of PVI's prognostic role. Quantifying its impact relative to these markers could strengthen its utility in clinical decision-making.

In conclusion, this study makes an important contribution to the literature by elucidating the role of PVI in breast cancer prognosis. Further integration of PVI into prognostic assessments and a more detailed exploration of its molecular associations could yield significant clinical benefits. We congratulate the authors once again on this noteworthy research and wish them continued success.

Sincerely,

Ethics

Financial Disclosure: The author declared that this study has received no financial support.

REFERENCE

1. Çalım Gürbüz B, Söylemez Akkurt T, Eren H, İzol Özmen H, Şen E, Pehlivanoğlu B. Perivascular invasion: a promising prognostic parameter for breast cancer. Medeni Med J. 2024;39:302-8.

DOI: 10.4274/MMJ.galenos.2025.75570
Medeni Med J 2025;40:33-34

Letter to the Editor

Correspondence on Effect of Different Doses of Sugammadex on Recovery and Hemodynamic Parameters in Reversing Neuromuscular Blockade in Patients Undergoing Electroconvulsive Therapy

"Elektrokonvülsif Tedavi Uygulanan Hastalarda Nöromusküler Blokajın Geri Döndürülmesinde Sugammadeksin Farklı Dozlarının Derlenme ve Hemodinamik Parametrelere Etkisi" Konulu Yazışma

Ahmet Ridvan DOGAN

Sakarya Training and Research Hospital, Clinic of Anesthesiology and Reanimation, Sakarya,Türkiye

Keywords: Sugammadex, cost analysis, anesthesia
Anahtar kelimeler: Sugammadex, maliyet analizi, anestezi

Dear Editor,

We read with great interest the article titled "Effects of Different Sugammadex Dosages on Recovery Times and Hemodynamic Parameters During Electroconvulsive Therapy" by Arslan et al.[1] in Medeniyet Medical Journal. The study provides valuable insight into optimizing neuromuscular blockade reversal during electroconvulsive therapy (ECT). However, we would like to highlight two critical points that warrant further discussion.

Firstly, the authors conclude that 3 mg/kg sugammadex is cost-effective compared to 2 mg/kg, as it results in a shorter recovery time. However, no formal cost-effectiveness analysis was conducted. Determining cost-effectiveness requires a comprehensive economic evaluation, including drug costs, total hospital stay, and potential complications. Without such an analysis, it remains unclear whether the additional cost of the higher dose is justified by its clinical benefits[2,3].

Secondly, while the study includes patients with different psychiatric diagnoses (bipolar disorder, major depression, psychosis), it does not analyze whether psychiatric conditions impact neuromuscular blockade reversal and recovery times. Given that psychiatric patients are frequently on psychotropic medications that influence brain metabolism, their recovery from anesthesia may vary[4]. Previous studies suggest that central nervous system pharmacodynamics differ among psychiatric populations, potentially affecting their anesthetic emergence[5]. Investigating whether different psychiatric disorders influence recovery times would provide valuable clinical insights and support individualized anesthesia management in ECT patients.

Address for Correspondence: A.R. Dogan, Sakarya Training and Research Hospital, Clinic of Anesthesiology and Reanimation, Sakarya,Türkiye
E-mail: a.ridvandogan@gmail.com **ORCID ID:** orcid.org/0000-0002-5481-8882

Cite as: Doğan AR, Correspondence on "effect of different doses of sugammadex on recovery and hemodynamic parameters in reversing neuromuscular blockade in patients undergoing electroconvulsive therapy". Medeni Med J. 2025;40:33-34

Received: 03. February 2025
Accepted: 11 February 2025
Published: 28 March 2025

We appreciate the authors' contribution to this important topic and look forward to further clarification regarding these issues. Addressing these concerns may help refine the clinical applicability of sugammadex dosing in psychiatric patients undergoing ECT.

Ethics

Conflict of Interest: The author have no conflict of interest to declare.

Financial Disclosure: The author declared that this study has received no financial support.

REFERENCES

1. Arslan K, Kucuksarac G, Cetin Arslan H, Aydin E, Sahin AS. Effect of different doses of sugammadex on recovery and hemodynamic parameters in reversing neuromuscular blockade in patients undergoing electroconvulsive therapy. Medeni Med J. 2024;39:16-23.
2. Carron M, Baratto F, Zarantonello F, Ori C. Sugammadex for reversal of neuromuscular blockade: a retrospective analysis of clinical outcomes and cost-effectiveness in a single center. Clinicoecon Outcomes Res. 2016;8:43-52.
3. De Robertis E, Zito Marinosci G, Romano GM, et al. The use of sugammadex for bariatric surgery: analysis of recovery time from neuromuscular blockade and possible economic impact. Clinicoecon Outcomes Res. 2016;8:317-22.
4. Naskar Chandrima, Grover Sandeep. Psychotropic medications around perioperative period: how to go about?. Journal of SAARC Psychiatric Federation. 2023;1:11-21
5. Fleisher LA. Preoperative evaluation. Anesthesiol Clin N Am. 2004;22:xi–xii.

DOI: 10.4274/MMJ.galenos.2025.33667
Medeni Med J 2025;40:35-36

Response to the Letter to the Editor Regarding Our Research Article on "Effect of Different Doses of Sugammadex on Recovery and Hemodynamic Parameters in Reversing Neuromuscular Blockade in Patients Undergoing Electroconvulsive Therapy"

"Elektrokonvülsif Tedavi Uygulanan Hastalarda Nöromusküler Blokajın Geri Döndürülmesinde Sugammadeksin Farklı Dozlarının Derlenme ve Hemodinamik Parametrelere Etkisi" Konulu Araştırma Makalemize İlişkin Editöre Mektuba Yanıt

Kadir ARSLAN, Ayca Sultan SAHIN

University of Health Sciences Türkiye, Kanuni Sultan Süleyman Training and Research Hospital, Clinic of Anesthesiology and Reanimation, Istanbul, Türkiye

Keywords: Electroconvulsive therapy, neuromuscular blocking agents, rocuronium, sugammadex, anesthesia recovery
Anahtar kelimeler: Elektrokonvülsif tedavi, nöromusküler bloker ajanlar, rokuronyum, sugammadeks, anestezi derlenmesi

Dear Editor,

We want to thank our readers for their interest in our research article on the recovery and hemodynamic parameters of different sugammadex doses (2 mg/kg and 3 mg/kg) in patients undergoing electroconvulsive therapy (ECT)[1]. The answers to the questions asked about our article are provided below.

First, sugammadex has made a breakthrough in the rapid and safe reversal of neuromuscular blockade. However, it is more costly than cholinesterase inhibitors used to reverse neuromuscular blockade. The effects of high doses of sugammadex, such as 8 mg/kg and 16 mg/kg, on recovery in ECT procedures have been investigated in the literature[2,3]. In our study, both 2 mg/kg and 3 mg/kg doses were effective and safe. In addition, it was determined that the 3 mg/kg dose provided faster recovery compared to the 2 mg/kg dose. As you stated, determining cost-effectiveness requires various evaluations, including drug cost, total hospital stay, and complications, but this is not the purpose of our study. No significant complications were observed in the patients included in the study other than hemodynamic changes that could be resolved with short-term interventions. In conclusion, as demonstrated in our study, low sugammadex doses are low-cost and safe in the recovery from anesthesia, however, comprehensive studies are needed regarding cost-effectiveness.

Address for Correspondence: Kadir Aslan, University of Health Sciences Türkiye, Kanuni Sultan Süleyman Training and Research Hospital, Clinic of Anesthesiology and Reanimation, Istanbul, Türkiye
E-mail: kadir.arslan@sbu.edu.tr **ORCID ID:** orcid.org/0000-0003-4061-0746

Cite as: Arslan K, Sahin AS. Response to the letter to the editor regarding our research article on "effect of different doses of sugammadex on recovery and hemodynamic parameters in reversing neuromuscular blockade in patients undergoing electroconvulsive therapy". Medeni Med J. 2025;40:35-36

Received: 09 February 2025
Accepted: 11 February 2025
Epub: 14.03.2025
Published: 28 March 2025

Secondly, we observed that approximately one in three patients in our study had bipolar disorder, one in three had major depression and depressive disorders, and one in three had psychosis, schizophrenia, and schizoaffective disorders. As you rightly pointed out, the recovery may vary depending on the diagnosis, and the drugs used in treatment. In our hospital practice, we did not find significant differences in recovery among patients with different diagnoses when using low-dose propofol-rocuronium for induction and 2-3 mg/kg sugammadex for reversal. However, we agree that further studies are necessary to fully understand this complex relationship.

We appreciate your interest in our research.

Ethics

Author Contributions

Concept: K.A., A.S.S., Design: K.A., A.S.S., Literature Search: K.A., A.S.S., Writing: K.A.

Conflict of Interest: The authors have no conflict of interest to declare.

REFERENCES

1. Arslan K, Kucuksarac G, Cetin Arslan H, Aydin E, Sahin AS. Effect of different doses of sugammadex on recovery and hemodynamic parameters in reversing neuromuscular blockade in patients undergoing electroconvulsive therapy. Medeni Med J. 2024;39:16-23.
2. Karahan MA, Büyükfırat E, Binici O, et al. The the effects of rocuronium-sugammadex on fetomaternal outcomes in pregnancy undergoing electroconvulsive therapy: a retrospective case series and literature review. Cureus. 2019;11:e4820.
3. Kadoi Y, Hoshi H, Nishida A, Saito S. Comparison of recovery times from rocuronium-induced muscle relaxation after reversal with three different doses of sugammadex and succinylcholine during electroconvulsive therapy. J Anesth. 2011;25:855-859.

Original Articles

Case Report

Letters to the Editor